AIMS Energy, 12(1): 84–118.
DOI: 10.3934/energy.2024005
Received: 02 October 2023
Revised: 18 December 2023
Accepted: 19 December 2023
Published: 02 January 2024

http://www.aimspress.com/journal/energy

Research article

Hybrid adaptive dwarf mongoose optimization with whale optimization algorithm for extracting photovoltaic parameters

Shijian Chen[1], Yongquan Zhou[2,*] and Qifang Luo[1,2]

[1] College of Artificial Intelligence, Guangxi Minzu University, Nanning 530006, China
[2] Guangxi Key Laboratories of Hybrid Computation and IC Design Analysis, Nanning 530006, China

*** Correspondence:** Email: zhouyongquan@gxun.edu.cn; Tel: +8613607882594; Fax: +867713265523.

Abstract: This article proposed adaptive hybrid dwarf mongoose optimization (DMO) with whale optimization algorithm (DMOWOA) to extract solar cell model parameters. In DMOWOA, the whale optimization algorithm (WOA) is used to enhance the capability of DMO in escaping local optima, while introducing inertial weights to achieve a balance between exploration and exploitation. The DMOWOA performances are tested through the solving of the single diode model, double diode model, and photovoltaic (PV) modules. Finally, the DMOWOA is compared with six well-known algorithms and other optimization methods. The experimental results demonstrate that the proposed DMOWOA exhibits remarkable competitiveness in convergence speed, robustness, and accuracy.

Keywords: parameters extraction; photovoltaic models; dwarf mongoose optimization; whale optimization algorithm; hybrid metaheuristic algorithm

1. Introduction

In consideration of the increasingly severe energy crisis and environmental pollution, renewable energy has garnered significant attention and recognition [1]. The renewable and emission-free characteristics of solar energy have garnered extensive attention, rendering it a subject of great significance in the academic community [2,3]. The photovoltaic system, serving as a solar energy-to-electricity conversion system, assumes a pivotal role within the power grid [4]. For the PV models [5], the single-diode and double-diode models are the most frequently employed in practice. The design and evaluation of photovoltaic systems rely heavily on the precision of parameters such

as current and resistance, which play a pivotal role [6]. The photovoltaic parameter extraction is performed within a simulated operational environment of an authentic photovoltaic system, where the current-voltage data is measured under all operational conditions of the actual photovoltaic system [7,8]. Therefore, it is extremely significant to extract PV model parameters accurately, quickly, and reliably.

In recent years, photovoltaic parameter extraction has emerged as a prominent research area, with numerous optimization methods proposed to address this issue [9]. These methods are analytical methods [10] and numerical approaches [11]. The implementation of analytical methods is straightforward, involving the analysis of mathematical equations to address problems. However, analytical methods heavily rely on selected values and inaccurate choices can result in flawed models. The field of numerical methods can be categorized into deterministic approaches and metaheuristic algorithms. Deterministic methods, such as the Newton-Raphson method [12], Lambert W function [13], Gauss-Seidel method [14], and iterative curve fitting [15], are commonly employed. Deterministic methods exhibit excessive reliance on initial values and are prone to falling into local optima. Metaheuristic algorithms are a general class of heuristic algorithms that do not rely on domain-specific knowledge but provide a general framework for searching the solution space of a problem to find an approximately optimal solution. Metaheuristic algorithms often meet some requirements of the search process, and then the heuristic algorithm implemented according to these requirements is called a metaheuristic algorithm. Many metaheuristic algorithms are inspired by some random phenomena in nature. Metaheuristic methods exhibit flexibility in the objective function and initial values, making them easily implementable. The inspiration for the mutation, crossover, and selection strategies of differential evolution comes from the theory of evolution in nature. Chaotic local search based differential evolution algorithms use the chaotic local search (CLS) mechanism to avoid premature convergence of evolutionary algorithms [16]. The non-dominated evolutionary optimization strategy based on covariance matrix adaptation (CMA-ES) is an evolutionary optimization strategy aimed at reducing the number of iterations required to converge to the optimal solution [17]. The Bayesian optimization framework is an excellent algorithm that considers heteroscedastic noise to adjust hyperparameters in control problems [18]. Consequently, metaheuristic algorithms find extensive applications in optimization problems across diverse domains. Numerous scholars have employed meta-heuristic techniques for addressing the challenge of parameter extraction in photovoltaic modeling, such as genetic algorithm (GA) [19], differential evolution (DE) [20], particle swarm optimization (PSO) [21], simulated annealing algorithm (SA) [22], moth-flame optimization [23], artificial bee colony algorithm (ABC) [24], teaching-based optimization algorithm (TLBO) [25], JAYA [26], etc. Many scholars have proposed improved algorithms to solve this problem, as reviewed below.

In [27], an improved PSO incorporating a cross-sorting and dynamic population reduction strategy is proposed for extracting photovoltaic parameters. In [28], an improved PSO based on an adaptive mutation strategy is proposed, which can avoid premature phenomena and accurately extract photovoltaic parameters. In [29], an improved DE to identify photovoltaic parameters under all conditions. In [30], a hybrid algorithm of DE/WOA is proposed, which combines exploration of DE and exploitation of WOA and can accurately extract photovoltaic parameters. In [31], a novel formulation is proposed for the computation of the scale factor and crossover rate, thereby enhancing the performance of adaptive differential evolution through its implementation. In [32], the present study proposes a novel teaching-learning-based artificial bee colony algorithm, which combines the

advantages of the teaching-learning-based optimization algorithm and the artificial bee colony algorithm, aiming to effectively extract photovoltaic parameters. In [33], an enhanced and simplified teach-learn optimization algorithm (STLBO) is proposed for parameter identification in proton exchange membrane (PEM) fuel cells and photovoltaic models. In [34], introduces a novel approach, namely the generalized oppositional teaching-learning-based optimization, for parameter extraction of photovoltaic models. In [35], an improved JAYA algorithm is proposed to effectively identify the parameters of a PV mode. In [36], the individual is quantified by probability, and then the evolutionary strategy is selected adaptively based on probability. A performance-guided JAYA is proposed to identify PV parameters. In [37], for accurate extract photovoltaic parameters, a multiple learning backtracking search algorithm is proposed. In [38], a memory-based improved gorilla troop optimizer is proposed, incorporating the exploration gorilla adaptive mutation mechanism (EGAMM) and gorilla memory saving technology. This algorithm effectively parameters the identification of photovoltaic models. In [39], introduces an enhanced whale optimization algorithm that incorporates two prey search strategies for precise extraction of photovoltaic parameters. In [40], introduces a novel chaotic whale optimization algorithm, which primarily employs chaotic mapping techniques to automatically compute and adapt internal parameters. This algorithm is effective in the precise extraction of photovoltaic parameters. In [41], proposes an improved pigeon-inspired optimization (PIO) algorithm based on the Taguchi method for the extraction of photovoltaic parameters. Simulation results show that the proposed algorithm is superior to the comparison algorithm. In [42], a two-phase quasi-affine transformation evolution with feedback (tfQUATRE) algorithm was proposed to extract PV parameters. This algorithm improves the ability of exploration and development by adjusting the search trend in different stages. Using historical populations as a form of feedback to guide the search for promising areas, maintain population diversity, and improve exploration ability. The experimental results show that the algorithm has strong competitiveness. In [43], propose a scale-free network-based differential evolution method. This method is based on the scale-free network-based population structure and a mutation operator that utilizes the neighborhood information provided by the scale-free structure. The experimental results indicate that this method can efficiently and reliably extract photovoltaic parameters. In [44], propose a differential evolution variant (PDcDE) to tackle the parameter estimation of solar PV models. This method uses an auto-controlled population strategy to adjust the population size during a search process, setting the diversity control parameters for determining the scaling factor and avoiding local optima through reverse search. In [45], a directional permutation differential evolution algorithm (DPDE) is proposed to tackle the parameter estimation of several kinds of solar PV models. DPDE utilizes the information generated by the search population and differential vector direction and has a strong global search ability to jump out of local optima.

These methods play a crucial role in PV model parameter extraction. However, owing to the multimodal characteristics inherent in the PV model, numerous existing methodologies are susceptible to encountering local optima during the parameter extraction process. There is still significant potential for enhancing the convergence speed and accuracy, particularly in the double diode model (DDM). Therefore, additional exploration of alternative methods is necessary for effective PV model parameter extraction.

The term “hybrid technology” refers to the amalgamation of two or more algorithms, harnessing their respective strengths to yield a novel algorithm that outperforms any single algorithm [46]. According to hybrid technology, the present study proposes a hybrid algorithm integrating dwarf

mongoose optimization algorithm (DMO) and WOA. Dwarf mongoose optimization algorithm [47] is a swarm intelligence based metaheuristic algorithm, proposed in 2022 by Jeffrey et al. The algorithm models the foraging behavior of a population of dwarf mongooses, incorporating three social groups: the alpha group, the babysitter group, and the scout group. This algorithm considers the entire family as a unit for foraging activities, with the female chief leading the initiation of foraging tasks and making decisions regarding path selection, distance covered, and choice of sleeping mounds. Whale optimization algorithm [48] is a population-based metaheuristic algorithm, which was proposed by Mirjalili in 2016 and has been widely applied to solve various optimization problems. The algorithm mainly simulates the collective behavior of humpback whales, providing a novel method for problem-solving. In this paper, a hybrid algorithm of dwarf mongoose optimization algorithm and whale optimization algorithm is proposed. The primary improvement lies in synergizing the strengths of DMO and WOA to enhance the algorithm's capability to escape local optima and expedite convergence speed. The algorithm incorporates adaptive weights to effectively balance the trade-off between exploration and exploitation abilities. DMOWOA has a strong ability to jump out of local optimal and fast convergence. The novelty of DMOWOA is that the search phase of the algorithm is divided into two stages, which make full use of the exploration ability of DMO and the exploitation ability of WOA. The proposed algorithm is employed to solve various photovoltaic models to validate its performance. Experimental results show that the proposed algorithm has excellent performance and competitiveness for the extraction of photovoltaic parameters.

The main contributions of this paper are:

(1) A hybrid metaheuristic DMOWOA optimization algorithm is proposed for extracting photovoltaic model parameters.

(2) The DMOWOA used a mixture of DMO's Alpha group search stage, scout group search stage, and WOA's Bubble-net attacking method to look for optimal fitness. Chaotic adaptive weights are introduced to balance exploration and exploitation.

(3) The DMOWOA algorithm is employed to solve five PV models, and the obtained results are compared with those achieved by DMO, WOA, and those reported in the existing literature.

The rest of the paper is organized as follows: Section 2 explains the mathematical formula of the photovoltaic model. Section 3 introduces basic DMO and WOA. Section 4 explains the hybrid algorithm DMOWOA. Section 5 presents the experimental analysis and results of different PV models. Finally, Section 6 gives the conclusion.

2. Problem model

This section presents the prevalent models utilized in photovoltaic systems, including the single diode model (SDM), double diode model (DDM), and photovoltaic module based on SDM. Additionally, the objective function is introduced.

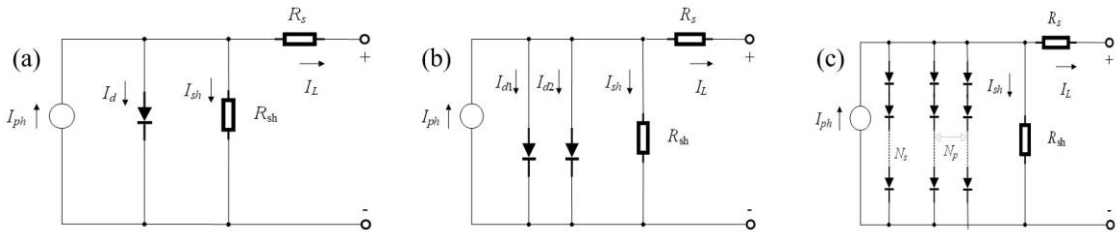

Figure 1. Equivalent circuit: (a) SDM, (b) DDM, and (c) PV module.

2.1. Single diode model

Figure 1(a) shows the equivalent circuit diagram of the single diode model. The figure shows that SDM consists of a diode, a photocurrent source, and two resistors. The mathematical model is as follows [49]:

$$\boldsymbol{I_o = I_{ph} - I_d - I_{sh}} \tag{1}$$

where I_{ph}, I_d, and I_{sh} are the photocurrent, diode current, and shunt resistance current, respectively.

The mathematical model of I_d and I_{sh} is as follows:

$$I_d = I_{sd}(\exp(\frac{V + IR_s}{aV_t}) - 1) \tag{2}$$

$$I_{sh} = \frac{V + IR_s}{R_{sh}} \tag{3}$$

where I_{sd}, V, R_s, and R_{sh} are the diode reverse saturation current, battery output voltage, series resistance, and shunt resistance, respectively.

The mathematical model of V_t is as follows:

$$V_t = \frac{k \cdot T}{q} \tag{4}$$

where k (= 1.3806503 × 10^{-23} J/K), T, and q (= 1.60217646 × 10^{-19} C) are Boltzmann's constant, the temperature in Kelvin, and the charge of the electron, respectively.

In summary, Eq (1) can be expressed as follows:

$$I_o = I_{ph} - I_{sd}(\exp(\frac{V + IR_s}{aV_t}) - 1) - \frac{V + IR_s}{R_{sh}} \tag{5}$$

In Eq (5), there are five unknown photovoltaic parameters (I_{ph}, I_{sd}, R_s, R_{sh}, and a) that need to be extracted. The effective operation of photovoltaic systems depends on these parameters.

2.2. Double diode model

The double diode model is one of the most commonly used PV models due to its simplicity and accuracy. It consists of a photocurrent source, two diodes, and two resistors, among which the two diodes are in a parallel state. Figure 1(b) shows its equivalent circuit diagram. The mathematical model of DDM is as follows [50]:

$$I_o = I_{ph} - I_{d1} - I_{d2} - I_{sh} \tag{6}$$

where I_{d1} and I_{d2} are the currents of two diodes in parallel. Their mathematical models are as follows:

$$I_{d1} = I_{sd1}(\exp(\frac{V + IR_s}{a_1 V_t}) - 1) \tag{7}$$

$$I_{d2} = I_{sd2}(\exp(\frac{V + IR_s}{a_2 V_t}) - 1) \tag{8}$$

where I_{sd1} and I_{sd2} are the saturation current at the two diodes, respectively, and a_1 and a_2 are ideal factors for both diodes.

In summary, Eq (6) can be expressed as follows:

$$I_o = I_{ph} - I_{sd1}(\exp(\frac{V + IR_s}{a_1 V_t}) - 1) - I_{sd2}(\exp(\frac{V + IR_s}{a_2 V_t}) - 1) - \frac{V + IR_s}{R_{sh}} \tag{9}$$

The formula reveals the presence of seven unknown parameters（I_{ph}, I_{sd1}, I_{sd2}, R_s, R_{sh}, a_1, and a_2）within the DDM model that necessitate extraction.

2.3. Photovoltaic module

The PV module is composed of multiple SDMs in series or parallel [51]. The mathematical model of the PV module is as follows:

$$I_o = I_{ph}N_p - I_{sd}N_p(\exp(\frac{V + IR_sN_s}{a_1 N_s V_t}) - 1) - \frac{V + IR_sN_s / N_p}{R_{sh}N_s / N_p} \tag{10}$$

where N_s and N_p are the number of cells in series and parallel, respectively. In this paper, the value of N_p is set to 1. In summary, Eq (10) can be expressed as follows:

$$I_o = I_{ph}N_p - I_{sd}(\exp(\frac{V + IR_sN_s}{a_1 N_s V_t}) - 1) - \frac{V + IR_sN_s}{R_{sh}N_s} \tag{11}$$

According to Eq (11), there are five unknown parameters (I_{ph}, I_{sd}, R_s, R_{sh}, and a) in the PV model module that need to be extracted.

2.4. Objective function

The optimal solution to the parameter extraction problem is to minimize the difference between the simulated current data and the measured current data. The root means square error (RMSE) is used for measurement error [52,53]. Therefore, the mathematical modeling of the PV model is as follows:

$$RMSE(X) = \sqrt{\frac{1}{N}\sum_{k=1}^{N} f(V_k, I_k, X)^2} \tag{12}$$

where N represents the number of experimental data. The objective function of the single diode model is as follows:

$$\begin{cases} f(V,I,X) = I_{ph} - I_{sd}(\exp(\frac{V+IR_s}{aV_t}) - 1) - \frac{V+IR_s}{R_{sh}} - I_o \\ X = \{I_{ph}, I_{sd}, R_s, R_{sh}, a\} \end{cases} \tag{13}$$

The objective function of the double diode model is as follows:

$$\begin{cases} f(V,I,X) = I_{ph} - I_{sd1}(\exp(\frac{V+IR_s}{a_1V_t}) - 1) - I_{sd2}(\exp(\frac{V+IR_s}{a_2V_t}) - 1) - \frac{V+IR_s}{R_{sh}} - I_o \\ X = \{I_{ph}, I_{sd1}, I_{sd2}, R_s, R_{sh}, a_1, a_2\} \end{cases} \tag{14}$$

The objective function of the PV module is as follows:

$$\begin{cases} f(V,I,X) = I_{ph}N_p - I_{sd}(\exp(\frac{V+IR_sN_s}{a_1N_sV_t}) - 1) - \frac{V+IR_sN_s}{R_{sh}N_s} - I_o \\ X = \{I_{ph}, I_{sd}, R_s, R_{sh}, a\} \end{cases} \tag{15}$$

3. Proposed hybrid DMO and WOA (DMOWOA)

3.1. DMO

The DMO [47] algorithm is a population-based metaheuristic algorithm proposed by Jeffrey O. Agushaka et al. The algorithm splits the mongoose population into three different groups: the alpha group, the scout group, and the babysitter group. Under the guidance of a female leader, the entire population collaboratively forages as a cohesive unit. In case the alpha group fails to locate food, an exchange occurs between members of the alpha and the babysitter group. Consequently, members of the alpha group simultaneously engage in foraging activities while searching for a sleeping mound. DMO requires only one manually controlled parameter to reduce the complexity of the algorithm application. When the members of the Alpha group have insufficient abilities, they will exchange members of the alpha group and the babysitter group, which gives DMO the ability to maintain population diversity. The sleep mound mechanism can prevent algorithms from entering local optima.

3.1.1. Initialization

Initializes the DMO's mathematical model, as shown in Eq (16).

$$X = \begin{bmatrix} X_{1,1} & X_{1,2} & \cdots & X_{1,d-1} & X_{1,d} \\ X_{2,1} & X_{2,1} & \cdots & X_{2,d-1} & X_{2,d} \\ \vdots & \vdots & X_{i,j} & \vdots & \vdots \\ X_{N,1} & X_{N,2} & \cdots & X_{N,d-1} & X_{N,d} \end{bmatrix} \tag{16}$$

where X represents the candidate solution; $X_{i,j}$ represents the position of the ith mongoose in the jth dimension, and its mathematical model is shown in Eq (17); and N and d represent the population count and the dimension size for the problem, respectively.

$$X_{i,\,j} = unifrnd(lb, ub, d) \tag{17}$$

where *unifrnd* is used to generate uniformly distributed random numbers, *ub* and *lb* represent the upper and lower bounds for the given problem respectively, and *d* represents the dimension size of the problem.

3.1.2. Alpha group

The foraging route of the dwarf mongoose is determined by the female leader, who is generated in the alpha group. The probability of each female individual in the alpha group becoming a leader is determined by Eq (18).

$$\alpha = \frac{fit(i)}{\sum_{i=1}^{n} fit(i)} \tag{18}$$

where *fit(i)* represents the fitness value of the ith individual; n represents the number of individuals in the alpha group, $n = N - bs$; and bs represents the number of individuals in the babysitters group.

Foraging paths are chosen by the alpha females, and its mathematical model is as follows:

$$X_{i+1} = X_i + p \times peep \times (X_i - X_k) \tag{19}$$

where X_{i+1} represents the new food source location, X_i is the location of the ith individual, p represents the random number between [−1,1], *peep* is set to 2, and X_k is a random individual in the alpha group. The sleeping mound (sm_i) is the resting place of dwarf mongooses, and its mathematical model is as follows:

$$sm_i = \frac{fit(i+1) - fit(i)}{\max\left\{\left| fit(i+1), fit(i)\right|\right\}} \tag{20}$$

The mathematical model of the mean sleeping mound is as follows:

$$\varphi = \frac{\sum_{i=1}^{n} sm_i}{n} \tag{21}$$

3.1.3. Scout group

The individual members of the scout group will not return to their previous sleeping mound. This guarantees the algorithm's exploration ability. The mathematical model of the sleeping mound is as follows:

$$X_{i+1} = \begin{cases} X_i - C \times p \times r \times \left| X_i - \overrightarrow{M} \right| & if\ \varphi_{i+1} > \varphi_i \\ X_i + C \times p \times r \times \left| X_i - \overrightarrow{M} \right| & else \end{cases} \tag{22}$$

where X_{i+1} is the position of the next sleeping mound; C represents the parameter controlling the mobility of the mongoose population, which will linearly decrease with the number of iteration, as shown in Eq (23); p is a random number between [−1,1]; r represents a random number between [0,1]; M is the vector that determines the direction in which the mongoose moves to the new sleeping mound, expressed by Eq (24); and φ is represented by Eq (21).

$$C = (1 - \frac{t}{Max\_t})^{(2\frac{t}{Max\_t})} \tag{23}$$

where t represents the iteration number and Max_t represents the maximum iteration count.

$$\overrightarrow{M} = \sum_{i=1}^{n} \frac{X_i - sm_i}{X_i} \tag{24}$$

where n represents the number of members in the scout group, X_i represents the position of the ith individual, and sm_i is the value of the sleeping mound.

3.1.4. Babysitter group

The size of the babysitter group, typically consisting of subordinate individuals caring for their offspring, is determined based on the population size. This influences the algorithm by proportionally decreasing the alpha group's foraging potential over time. Parameter L resets the information about foraging locations for other members. The fitness weight of the babysitter is set to zero, which ensures the average weight of the alpha group in the next iteration is reduced, which means the group movement is hindered thereby, emphasizing exploitation.

3.2. WOA

WOA [48] is a population-based metaheuristic algorithm proposed by Mirjalili and Lewis in 2016. WOA encompasses three distinct mathematical models: encircling prey, bubble-net attacking method, and search for prey. The three population updating mechanisms of WOA are independent of each other, and the global exploration and local development processes in the optimization stage can be operated and controlled separately. WOA does not require parameter adjustment, which improves the efficiency of algorithm usage and reduces application difficulty.

3.2.1. Encircling prey

Whales can recognize prey and use cooperative strategies to encircle their targets. The mathematical model is as follows:

$$\vec{V} = \left| \vec{S} \times \overrightarrow{X^*}_t - \vec{X}_t \right| \tag{25}$$

$$\vec{X}_{t+1} = \overrightarrow{X^*}_t - \vec{A} \times \vec{V} \tag{26}$$

where X^* and X represent the current optimal solution and the position of individual whales respectively. The mathematical models of A and S are shown as follows:

$$\vec{A} = 2 \times \vec{a} \times \vec{r} - \vec{a} \tag{27}$$

$$\vec{S} = 2 \times \vec{r} \tag{28}$$

where a decreases from 2 to 0 during iteration and r represents the vector between [0,1].

3.2.2. Bubble-net attacking method

Spiral update position: the whales make a spiral motion, and the mathematical model is as follows:

$$\vec{X}_{t+1} = \overrightarrow{V'} \cdot e^{bl} \cdot \cos(2\pi l) + \overrightarrow{X^*}_t \tag{29}$$

where $\overrightarrow{V'} = \left| \overrightarrow{X^*}_t - \vec{X}_t \right|$ represents the distance between the ith whale and its prey, b is the constant that defines the shape of the logarithmic spiral, and l represents the random number between [−1,1].

The whale follows a spiral trajectory, gradually encircling its prey within a confined circumference. To simulate these concurrent actions effectively, assign equal probabilities to both the updates of the narrow circle and spiral models governing the whale's position. The mathematical representation is as follows:

$$\vec{X}_{t+1} = \begin{cases} \overrightarrow{X^*}_t - \vec{A} \times \vec{V} & if \ p < 0.5 \\ \overrightarrow{V'} \cdot e^{bl} \cdot \cos(2\pi l) + \overrightarrow{X^*}_t & if \ p \geq 0.5 \end{cases} \tag{30}$$

where p represents a random number between [0,1].

3.2.3. Search for prey

Whales hunt at random based on the location of their peers. When an individual hunts, it moves away from the reference whale in the population. The mathematical model of the random hunt phase is as follows:

$$\vec{X}_{t+1} = \overrightarrow{X_{rand}} - \vec{A} \cdot \vec{V} \tag{31}$$

$$\vec{V} = \left| \vec{S} \cdot \overrightarrow{X_{rand}} - \vec{X} \right| \tag{32}$$

where X_{rand} represents a random individual whale and $|A| \geq 1$ or $|A| < 1$.

4. Adaptive weighted DMO hybrid WOA

4.1. Adaptive weight

Inertial weight is used to balance global and local search [54]. During the early stage, global search can enhance the algorithm's efficacy in identifying the optimal solution. During the later stage, local search can enhance the exploitability of the algorithm and improve the accuracy of the solution. In this paper, the chaotic inertia weight is adopted [55,56], and the mathematical model is as follows:

$$w = (w_{\max} - w_{\min}) \times \frac{T - t}{T} + w_{\min} \times z \tag{33}$$

where w_{max} and w_{min} are 0.9 and 0.4 respectively, $z = 4z(1 - z)$, and the value range of z is [0,1]. Equation (19) will be substituted by Eq (34), and Eq (22) will be replaced by Eq (35).

$$X_{i+1} = X_i + w \times p \times peep \times (X_i - X_k) \tag{34}$$

$$X_{i+1} = \begin{cases} X_i - w \times C \times p \times r \times \left| X_i - \overrightarrow{M} \right| & if\ \varphi_{i+1} > \varphi_i \\ X_i + w \times C \times p \times r \times \left| X_i - \overrightarrow{M} \right| & else \end{cases} \tag{35}$$

Chaos inertial weight exhibits the characteristics of general inertial weight and chaos, which can better balance the global search and local search of the algorithm.

4.2. Hybrid DMOWOA method

Whale optimization algorithm [36] is a highly efficient algorithm that demonstrates exceptional capabilities in solving various optimization problems. It is worth noting that WOA's ability to exploit in the late stages of the algorithm is excellent. The proposed algorithm removes the babysitter mechanism from the DMO and lets the alpha group and the scout group run simultaneously. Make sure they are foraging and looking for a sleeping mound at the same time. During the $p < 0.5$ stage of WOA, if $|A| < 1$, the alpha group performs both foraging and sleep mound search, that is, Eq (26) of WOA will be replaced by the Eqs (34) and (35) of DMO. If $|A| \geq 1$, the scout group engages in foraging and sleep mound search, that is, Eq (26) of WOA will be replaced by Eqs (34) and (35) of the scout group. Mining for bubble network attack of WOA, namely the position of spiral update, when WOA is at $p \geq 0.5$ stage. The pseudo-code and flow chart of DMOWOA are shown in Algorithm 1 and Figure 2 respectively.

Algorithm 1. DMOWOA's pseudo-code.

Step 1. Initialization
Set the values of *Max_t*, *t*, *N*, *d*, *peep*, $w_{max,}$ $w_{min,}$ *A*, fit_best, *Xbest*, φ
Step 2. Main loop
while $t \leq Max\_t$
  Calculate the value of *C* using Eq (23) and *w* using Eq (33)
  for *i* = 1:*N*
  Calculate the value of *A* using Eq (27)
    for *j* = 1:*d*
      if $p < 0.5$
        if $|A| \geq 1$
          Calculate the position X_{i+1} using Eq (34) and φ_{i+1} using Eq (21)
          Calculate the X_{i+1}'fitness and update the fit_best
          if $\varphi_{i+1} > \varphi$
            Calculate the position X_{i+1} using Eq (35-1)
           else
            Calculate the position X_{i+1} using Eq (35-2)
          end
          Update the $\varphi = \varphi_{i+1}$
        end
        if $|A| < 1$
          Calculate the position X_{i+1} using Eq (34)
          Calculate the X_{i+1}'fitness and update the fit_best
          Calculate the φ_{i+1} using Eq (21)
          if $\varphi_{i+1} > \varphi$
            Calculate the position X_{i+1} using Eq (35-1)
          else
            Calculate the position X_{i+1} using Eq (35-2)
          end
          Update the $\varphi = \varphi_{i+1}$
        end
      if $p \geq 0.5$
        Calculate the position X_{i+1} using Eq (30-2)
      end
    end
  end
end while
Step 3. Return fit_best and *Xbest*

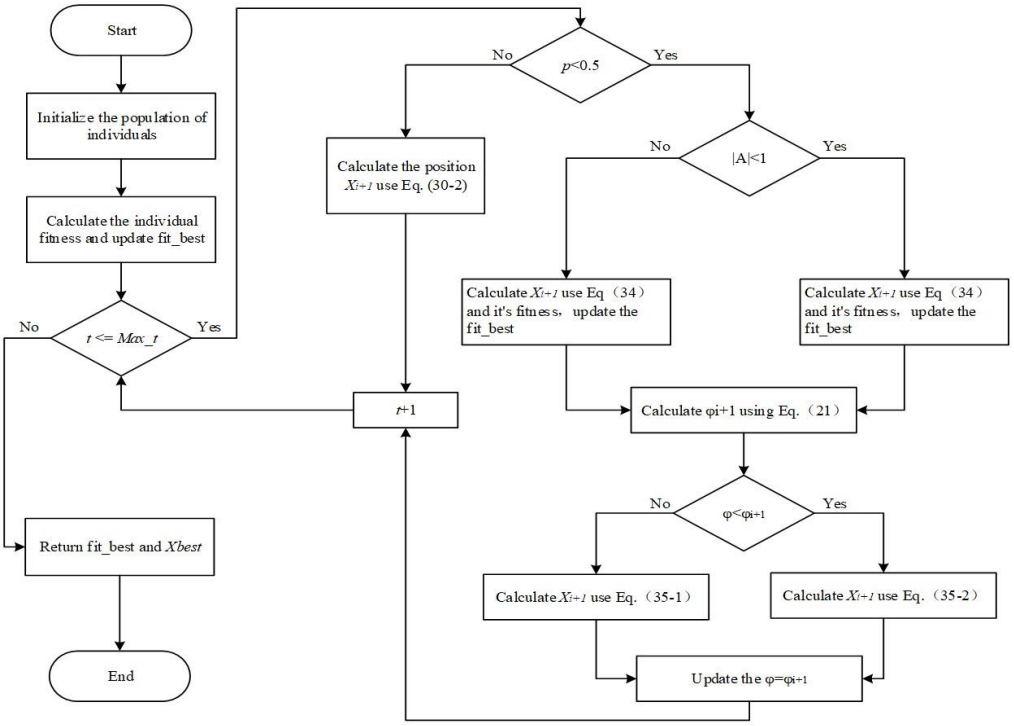

Figure 2. The flow diagram of DMOWOA.

4.3. Exploration and exploitation

Exploration and exploitation are the cornerstones of metaheuristic algorithms [57]. When achieving a balance between exploration and exploitation, algorithms can quickly converge during optimization. Effectively controlling the balance between exploration and exploitation is a challenging task. Representing the changing process of exploration and development is also important. According to [57], the current proportion of exploration and development can be determined based on the position between individuals. Its mathematical model is as follows:

$$Expa = (\frac{Dv}{Dv_{\max}}) \times 100\% \tag{36}$$

$$Expi = (\frac{|Dv - Dv_{\max}|}{Dv_{\max}}) \times 100\% \tag{37}$$

where *Expa* is the level of exploration, *Expi* is the level of exploitation, *Dv* is the dimension-wise diversity, and Dv_{max} is the maximum diversity value in the entire optimization process. The mathematical models of *Dv* and Dv_{max} are shown below:

$$Dv = \frac{1}{d}\sum_{1}^{d} Dv_j \tag{38}$$

$$Dv_j = \frac{1}{N}\sum_{1}^{N} |X_{i,j} - median(X_j)| \tag{39}$$

where $X_{i,j}$ represents the jth dimension of the ith individual, N is the population size, d is the dimension of the given problem, and $median(X_j)$ is the median value of the jth dimension in the whole population.

Figure 3 shows the variation process of exploration and development proportion when DMOWOA solves different photovoltaic models. As shown in the graph, DMOWOA has a fast convergence speed and stable changes in exploration and exploitation.

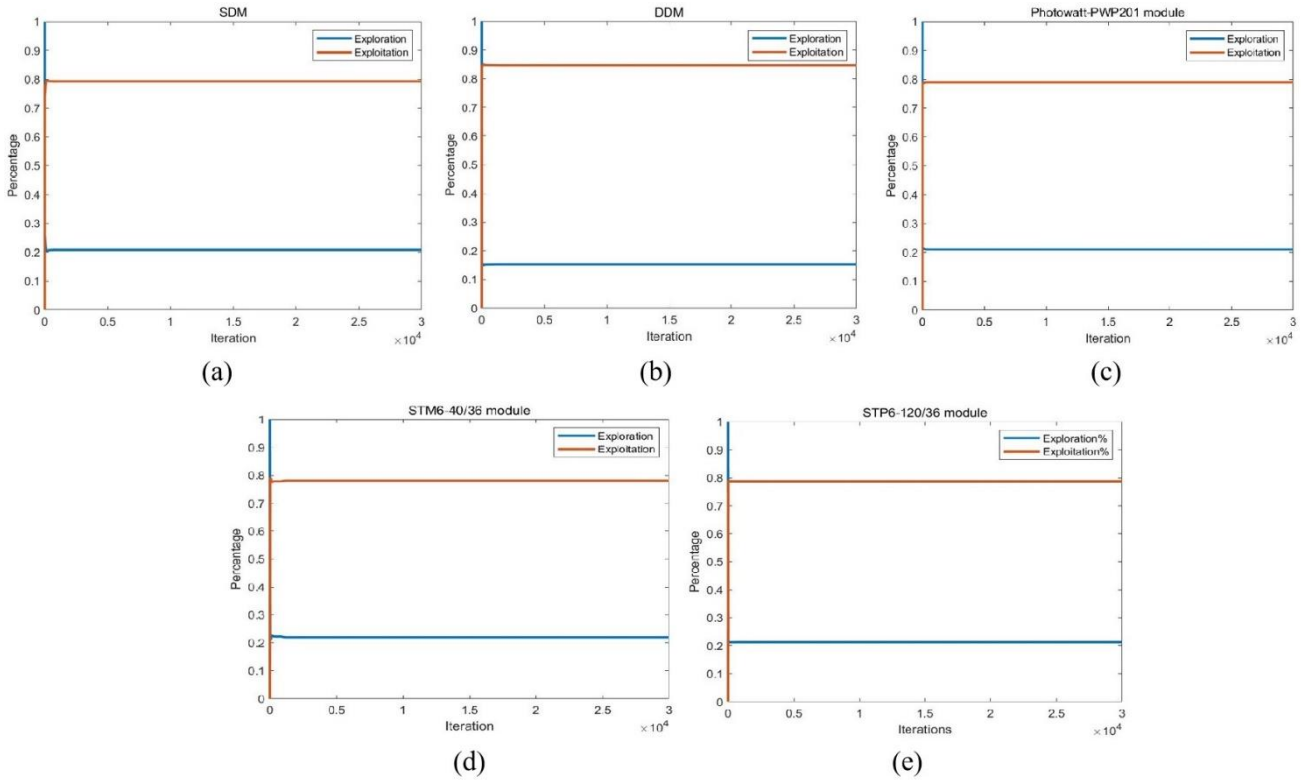

Figure 3. The percentage of exploration and exploitation: (a) single diode model, (b) double diode model, (c) Photowatt-PWP201 module, (d) STM6-40/36 module, and (e) STP6-120/36 module.

4.4. Computational complexity

The computational complexity of DMOWOA depends on the population size, the problem size, the number of iterations, the computation of the sleep mound search, and the computation of the fitness function. The computational complexity of the solution update process is $O(Max\_t \times d \times sm) + O(\text{CFE})$, including finding the best location, evaluating the next sleep hill, and updating the solution location for all solutions. The total number of iterations is Max_t, the dimension size of the given problem is d, CFE is the cost of function evaluation, and the population size is N. Therefore, the computational complexity of the proposed DMOWOA is $O(Max\_t \times d \times sm \times N + \text{CFE} \times N)$.

The detailed process of DMOWOA is shown in Algorithm 1 and Figure 2. At the beginning of optimization, individuals set out to search for food, and when $|A| \geq 1$, individuals will extensively search for food to determine its range. During subsequent foraging phases, individuals will search for food near the previous sleep mound to avoid reducing the efficiency of searching for food.

When |A| < 1, individuals will locate food within the determined range of food sources. To utilize the DMOWOA algorithm, it just needs to determine the population size and the maximum number of iterations.

5. Results and analysis

In this chapter, the DMOWOA is applied to extract three different PV models to verify the performance of the algorithm, including single diode, double diode, and PV modules. Current and voltage data of SDM and DDM [12] were measured on a commercial silicon R.T.C France solar cell with a diameter of 57 mm at 1000 W/m^2 at 33 ℃. PV modules include Photowatt-PWP201 [12], mono-crystalline STM6-40/36 [58], and poly-crystalline STP6-120/36 [58], and their respective current and voltage data can be found in their respective literature. Table 1 shows the value range of parameters of the PV model, which is consistent with the previous literature. The upper and lower bounds of the parameter values of the PV models are shown in Table 1.

To evaluate the performance of DMOWOA, compared DMOWOA with several established optimization algorithms including SA [22], DMO [47], WOA [48], DE [59], PSO [60], and GWO [64]. At the same time, it is compared with the algorithms proposed in other literature, including TLABC [32], GOTLBO [34], IJAYA [35], MLBSA [37], and IGBO [61], whose data is from their respective literature. The experimental conditions of all algorithms are run independently for 30 times, with the upper limit of 30000 for each iteration. Parameter configurations of the compared algorithms are provided in Table 2. In addition, this experiment uses MATLAB2021b for simulation experiments, and a Windows 10 64-bit operating system PC with Intel Core i7-9700 processor @3.00GHz and 16.0 GB RAM serves as the experimental platform.

Table 1. Upper and lower bounds for PV model parameters.

Parameter	SDM/DDM		Photowatt-PWP201		STM6-40/36		STP6-120/36	
	lb	*ub*	*lb*	*ub*	*lb*	*ub*	*lb*	*ub*
I_{ph}(A)	0	1	0	2	0	2	0	8
I_{sd}, I_{sd1}, I_{sd2}(μA)	0	1	0	50	0	50	0	50
R_s(Ω)	0	0.5	0	2	0	0.36	0	0.36
R_{sh}(Ω)	1	100	0	2000	0	1000	0	1500
a, a_1, a_2	1	2	1	50	1	60	1	50

Table 2. Parameter setting of compared algorithms.

Algorithms	Parameter setting
DMOWOA	N = 50
DMO	N = 50, bs = 3
PSO	N = 50, w = 0.729, c1 = 1.49445, c2 = 1.49445
GWO	N = 50, a = 2~0
SA	N = 50
DE	N = 50
WOA	N = 50, a = 2~0

5.1. Results on the SDM

Table 3 shows the parameters of SDM extracted by each algorithm. The minimum RMSE values in the table are shown in boldface type. Table 3 reveals that the DOMWOA, DMO, DE, MLBSA, and TLABC exhibit the optimal RMSE. WOA has the maximum RMSE. The accuracy of the extracted parameters increases as the RMSE decreases, as stated by [62]. The bar chart of SDM is shown in Figure 4. Therefore, the results of DMOWOA are more accurate than those of WOA, SA, PSO, GWO, GOTLBO, and IJAYA.

Table 3. SDM parameters are extracted from each algorithm.

Method	I_{ph} (A)	I_{sd} (μA)	R_s (Ω)	R_{sh} (Ω)	a	RMSE	Runtime (s)
DMOWOA	0.76077	0.32301	0.03637	53.71840	1.48118	**9.860219E-04**	**483.44**
DMO	0.76077	0.32306	0.03637	53.72317	1.48119	**9.860219E-04**	501.54
WOA	0.76147	0.29578	0.03658	44.37821	1.47253	1.107616E-03	532.68
DE	0.76077	0.32302	0.03637	53.71899	1.48118	**9.860219E-04**	531.65
SA	0.76069	0.38973	0.03562	59.42678	1.50032	1.049349E-03	1049.39
PSO	0.76077	0.32350	0.03637	53.75926	1.48133	9.860259E-04	513.35
GWO	0.76102	0.33113	0.03622	50.98459	1.48375	1.005399E-03	561.26
IGBO [61]	0.760776	0.323021	0.036377	53.718531	1.481184	**9.860219E-04**	NA
GOTLBO [34]	0.760780	0.331552	0.036265	54.115426	1.483820	9.87442E-04	NA
MLBSA [37]	0.760776	0.32302	0.036377	53.71852	1.481184	**9.8602E-04**	NA
TLABC [32]	0.76078	0.32302	0.03638	53.71636	1.48118	**9.86022E-04**	NA
IJAYA [35]	0.7608	0.3228	0.0364	53.7595	1.4811	9.8603E-04	NA

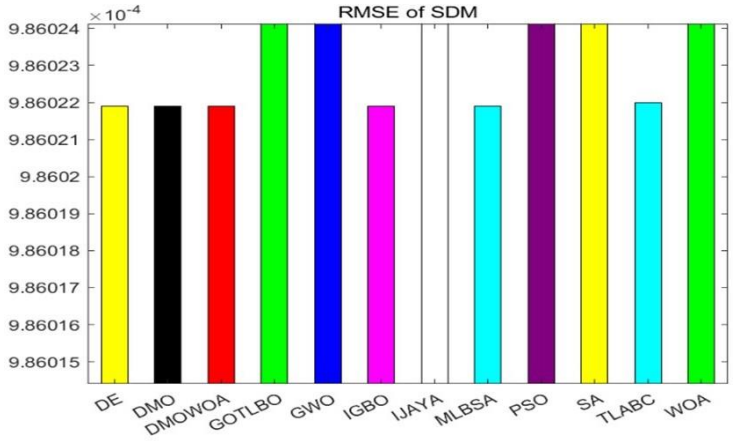

Figure 4. RMSE bar chart of SDM.

To further validate the accuracy of DMOWOA, Figure 5 plots the I-V and P-V curves of DMOWOA. Table 4 shows the integral absolute error (IAE) values. Figure 4 shows that the simulation results obtained using DMOWOA exhibit excellent agreement with the experimental measurements. In addition, according to Table 4, the IAE values of current are less than 2.51E-03, and the IAE values of voltage are less than 1.46E-02, thereby confirming the high precision of the parameters extracted by DMOWOA.

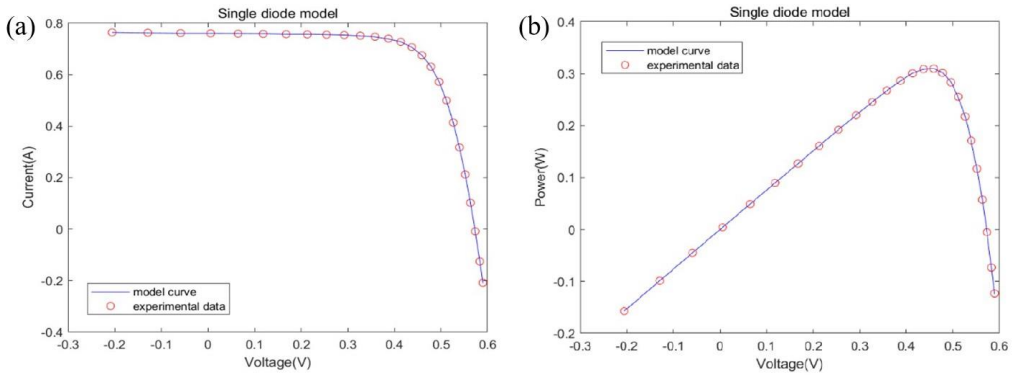

Figure 5. Comparison of experimental data and model data on SDM: (a) I-V curve, (b) P-V curve.

Table 4. SDM: IAE of DMOWOA.

Item	Model data		Experiment current data		Experiment power data	
	V_M (V)	I_M (A)	I_E (A)	IAE_I (A)	P_E (W)	IAE_P (W)
1	−0.2057	0.7640	0.764087182	0.00008718	−0.15717120	0.00001640
2	−0.1291	0.7620	0.762662561	0.00066256	−0.09845974	0.00008550
3	−0.0588	0.7605	0.761354779	0.00085478	−0.04476766	0.00005030
4	0.0057	0.7605	0.760153460	0.00034650	0.00433287	0.00000198
5	0.0646	0.7600	0.759054675	0.00094530	0.04903493	0.00006110
6	0.1185	0.7590	0.758041810	0.00095820	0.08982795	0.00011400
7	0.1678	0.7570	0.757091116	0.00009112	0.12703989	0.00001500
8	0.2132	0.7570	0.756140826	0.00085920	0.16120922	0.00018300
9	0.2545	0.7555	0.755086333	0.00041370	0.19216947	0.00010500
10	0.2924	0.7540	0.753663340	0.00033670	0.22037116	0.00009840
11	0.3269	0.7505	0.751390433	0.00089043	0.24562953	0.00029000
12	0.3585	0.7465	0.747353327	0.00085333	0.26792617	0.00031000
13	0.3873	0.7385	0.740116716	0.00161672	0.28664720	0.00063000
14	0.4137	0.7280	0.727381749	0.00061830	0.30091783	0.00025600
15	0.4373	0.7065	0.706972218	0.00047222	0.30915895	0.00021000
16	0.4590	0.6755	0.675279776	0.00022020	0.30995342	0.00010100
17	0.4784	0.6320	0.630757962	0.00124200	0.30175461	0.00059400
18	0.4960	0.5730	0.571928111	0.00107190	0.28367634	0.00053200
19	0.5119	0.4990	0.499606814	0.00060681	0.25574873	0.00031000
20	0.5265	0.4130	0.413648598	0.00064860	0.21778599	0.00034000
21	0.5398	0.3165	0.317509874	0.00100987	0.17139183	0.00055000
22	0.5521	0.2120	0.212154600	0.00015460	0.11713055	0.00008500
23	0.5633	0.1035	0.102250802	0.00124920	0.05759788	0.00070400
24	0.5736	−0.0100	−0.008718296	0.00128170	−0.00500081	0.00074000
25	0.5833	−0.1230	−0.125508482	0.00250850	−0.07320910	0.00146300
26	0.5900	−0.2100	−0.208473677	0.00152632	−0.12299947	0.00090053
SIAE				0.02152594		0.00874621

Note: SIAE: Sum of IAE.

5.2. Results on the DDM

This section presents and analyzes the experimental data of DDM. Table 5 shows the parameters of DDM extracted by each algorithm. The minimum RMSE value is indicated in boldface. Figure 6 shows the bar chart of DDM. As shown in Table 5, the RMSE of DMOWOA and MLBSA are the lowest, followed by IJAYA, GOTLBO, PSO, TLABC, DMO, DE, SA, and GWO. WOA has the highest RMSE.

Table 5. DDM parameters are extracted from each algorithm.

Method	I_{ph} (A)	I_{sd1} (μA)	I_{sd2} (μA)	R_s (Ω)	R_{sh} (Ω)	a_1	a_2	RMSE	Runtime (s)
DMOWOA	0.760784	0.223112	0.774202	0.03675	55.55108	1.44995	2	**9.824894E-04**	**501.87**
DMO	0.760745	0.268287	0.288613	0.03645	54.61122	1.47161	2	9.857786E-04	511.14
WOA	0.760737	0.681735	0.30963	0.03670	60.94388	1.331801	1.6412	1.11496E-03	542.06
DE	0.7607742	0.322691	0.598969	0.03637	53.72476	1.63652	1.4811	9.86023E-04	544.85
SA	0.7608018	0.162530	1	0.03714	55.35953	1.94119	1.4241	9.88079E-04	1135.89
PSO	0.760775	0.357170	0.274889	0.03653	54.57654	1.46751	2	9.835519E-04	538.62
GWO	0.7606555	0.204797	0.807745	0.03640	60.71382	1.90417	1.4460	1.01086E-03	521.41
IGBO [61]	0.76077	0.21969	0.11923	0.03643	53.86796	1.517865	1.4468	9.826373E-04	NA
GOTLBO [34]	0.76075	0.80019	0.22046	0.0368	56.07530	1.99997	1.44897	9.83177E-04	NA
MLBSA [37]	0.7608	0.22728	0.73835	0.0367	55.4612	1.4515	2	**9.8249E-04**	NA
TLABC [32]	0.76081	0.42394	0.24011	0.03667	54.66797	1.9075	1.4567	9.84145E-04	NA
IJAYA [35]	0.7601	0.00504	0.75094	0.0376	77.8519	1.2186	1.6247	9.8293E-04	NA

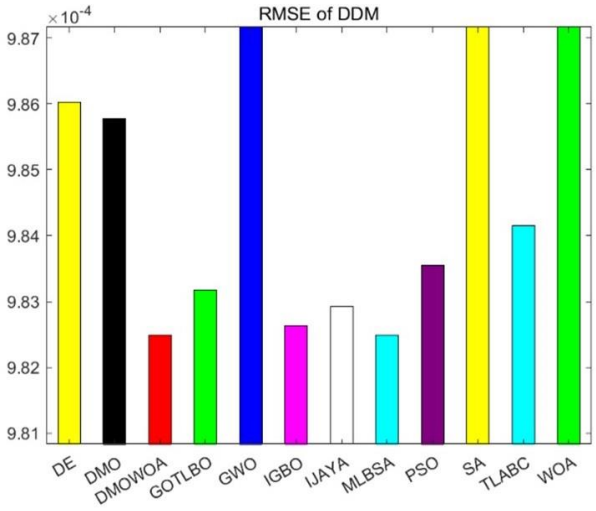

Figure 6. RMSE bar chart of DDM.

To validate the accuracy of DMOWOA, Figure 6 shows the I-V and P-V curves of DDM. Table 6 shows the IAE values for DDM. It can be observed from Figure 6 that the simulation results obtained using DMOWOA exhibit excellent agreement with the experimental measurements. Figure 7 further confirms the close match between DMOWOA's simulations and the model data. Furthermore,

according to Table 6, the current-related IAE values are all less than 2.51E-03, and the power-related IAE values are all less than 1.46E-01, thereby confirming the high precision of the parameters extracted by DMOWOA.

Table 6. DDM: IAE of DMOWOA.

Item	Model data		Experiment current data		Experiment power data	
	V_M (V)	I_M (A)	I_E (A)	IAE_I (A)	P_E (W)	IAE_P (W)
1	−0.2057	0.7640	0.763979398	0.00002060	−0.15715048	0.00000432
2	−0.1291	0.7620	0.762601709	0.00060170	−0.09845188	0.00007768
3	−0.0588	0.7605	0.761336799	0.00083679	−0.04476660	0.00004920
4	0.0057	0.7605	0.760174234	0.00032577	0.00433299	0.00000186
5	0.0646	0.7600	0.759109304	0.00089070	0.04903846	0.00005754
6	0.1185	0.7590	0.758124007	0.00087599	0.08983769	0.00010381
7	0.1678	0.7570	0.757191858	0.00019185	0.12705679	0.00003219
8	0.2132	0.7570	0.756247066	0.00075293	0.16123187	0.00016053
9	0.2545	0.7555	0.755180370	0.00031963	0.19219340	0.00008135
10	0.2924	0.7540	0.753724314	0.00027569	0.22038899	0.00008061
11	0.3269	0.7505	0.751399328	0.00089932	0.24563244	0.00029399
12	0.3585	0.7465	0.747299496	0.00079949	0.26790687	0.00028662
13	0.3873	0.7385	0.740006804	0.00150680	0.28660464	0.00058359
14	0.4137	0.7280	0.727242128	0.00075787	0.30086007	0.00031353
15	0.4373	0.7065	0.706846066	0.00034606	0.30910378	0.00015133
16	0.4590	0.6755	0.675208453	0.00029155	0.30992068	0.00013382
17	0.4784	0.6320	0.630761645	0.00123836	0.30175637	0.00059243
18	0.4960	0.5730	0.571998419	0.00100158	0.28371122	0.00049678
19	0.5119	0.4990	0.499711545	0.00071154	0.25580234	0.00036424
20	0.5265	0.4130	0.413739086	0.00073908	0.21783363	0.00038913
21	0.5398	0.3165	0.317550239	0.00105023	0.17141362	0.00056692
22	0.5521	0.2120	0.212124746	0.00012474	0.11711407	0.00006887
23	0.5633	0.1035	0.102162901	0.00133710	0.05754836	0.00075319
24	0.5736	−0.0100	−0.008792057	0.00120794	−0.00504312	0.00069288
25	0.5833	−0.1230	−0.125543076	0.00254308	−0.07322928	0.00148338
26	0.5900	−0.2100	−0.208367065	0.00163293	−0.12293657	0.00096343
SIAE				0.02127933		0.00878322

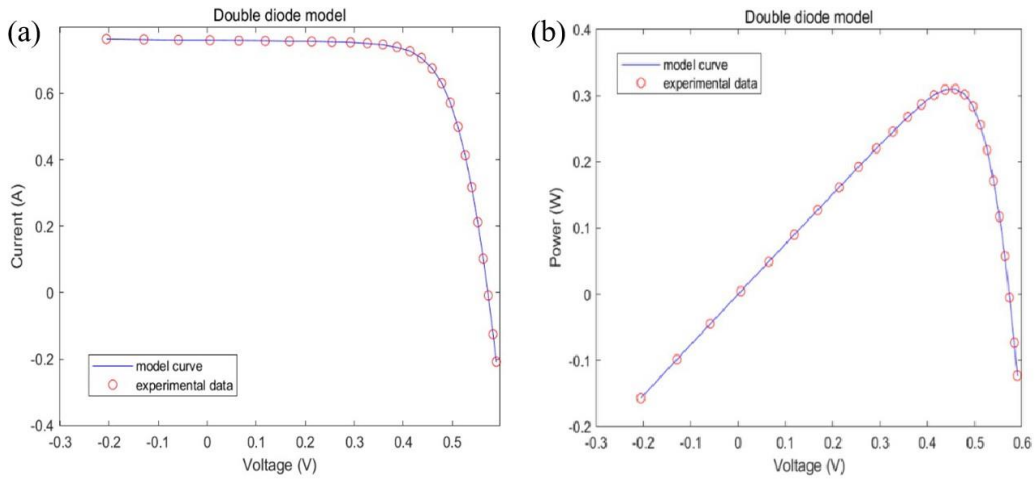

Figure 7. Comparison of experimental data and model data on DDM: (a) I-V curve, (b) P-V curve.

5.3. Results on photovoltaic modules

This section presents and analyzes the experimental results of three photovoltaic modules extracted by DMOWOA. Table 7 summarizes the experimental results of each algorithm for the Photowatt-PWP201 module, and Figure 8 is a bar chart of the results. As shown in Table 7, DMOWOA, MLBSA, TLABC, and IJAYA had the lowest RMSE values, followed by DMO, PSO, GOTLBO, and GWO. WOA had the highest RMSE value.

Table 7. Photowatt-PWP201 module parameters are extracted from each algorithm.

Method	I_{ph} (A)	I_{sd} (μA)	R_s (Ω)	R_{sh} (Ω)	a	RMSE	Runtime (s)
DMOWOA	1.030514	3.482239	1.201272	981.971946	48.642809	**2.425075E-03**	**488.08**
DMO	1.663914	1.735726	0.154112	573.027822	54.724284	2.425081E-03	507.10
WOA	1.026966	4.124698	1.189613	1953.97648	49.287535	2.604337E-03	529.81
DE	1.0305156	3.481452	1.201295	981.730091	48.641944	**2.425075E-03**	537.03
SA	1.0297633	3.985231	1.1871969	1153.36510	49.164517	2.453717E-03	1037.09
PSO	1.0305369	3.471742	1.2015711	978.090865	48.631283	2.425089E-03	520.57
GWO	1.0299345	4.035756	1.1853753	1136.06045	49.214774	2.460404E-03	557.67
IGBO [61]	1.030514	3.482264	1.201271	981.982332	48.642836	**2.425075E-03**	NA
GOTLBO [34]	1.030439	3.4573	1.201258	982.1211	48.61538	2.427130E-03	NA
MLBSA [37]	1.0305	3.4823	1.2013	981.9823	48.6428	**2.425075E-03**	NA
TLABC [32]	1.03056	3.4715	1.20165	972.93567	48.63131	**2.42507E-03**	NA
IJAYA [35]	1.030514	3.4822	1.201272	981.9763	48.64281	**2.425075E-03**	NA

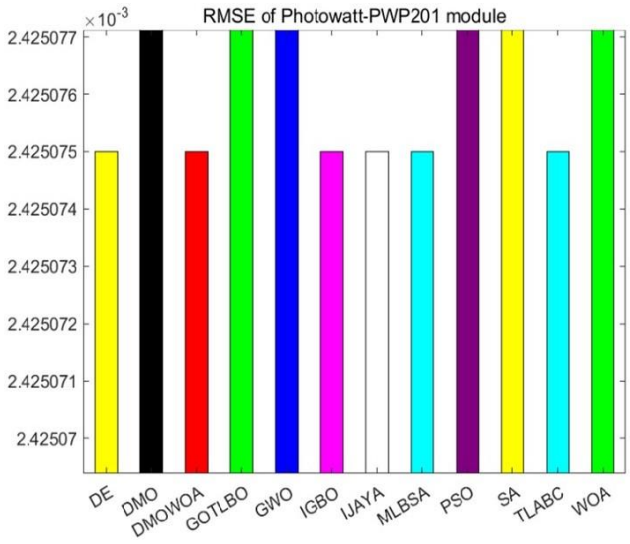

Figure 8. RMSE bar chart of Photowatt-PWP201 module.

For the STM6-40/36 module, Table 8 shows the parameters extracted by each algorithm, and Figure 9 is the bar chart of RMSE. As shown in Table 8, only DMOWOA, MLBSA, and TLABC achieved the lowest RMSE values. SA had the highest RMSE value.

Table 8. STM6-40/36 module parameters are extracted from each algorithm.

Method	I_{ph} (A)	I_{sd} (μA)	R_s (Ω)	R_{sh} (Ω)	a	RMSE	Runtime (s)
DMOWOA	1.6639047	1.7386536	0.1538559	573.417952	54.730897	**1.729814E-03**	**493.08**
DMO	1.6639143	1.7357265	0.1541121	573.027824	54.724282	1.729834E-03	509.05
WOA	1.6620926	2.0608957	0.1378843	663.11838	55.408003	1.884297E-03	524.98
DE	1.6639003	1.7416859	0.1536555	573.732383	54.737794	1.729815E-03	533.03
SA	1.6619204	3.8724258	0.0565242	775.104134	58.093992	2.572752E-03	991.59
PSO	1.6639057	1.7379582	0.1539021	573.347891	54.729314	**1.729814E-03**	510.36
GWO	1.6603481	3.3048336	0.0850471	860.127103	57.389381	2.494334E-03	570.67
IGBO[61]	1.663905	1.738653	0.153856	573.418117	54.730896	**1.729814E-03**	NA
GOTLBO[63]	1.663236	2.9641	0.002246	17.90892	1.581384	2.233818E-03	NA
MLBSA[27]	1.663905	1.7387	0.004274	15.92829	1.520303	**1.729814E-03**	NA
TLABC[27]	1.6639	1.7387	0.0043	15.9283	1.5203	**1.7298E-03**	NA
IJAYA[63]	1.6637	1.8353	0.0040	15.9449	1.5263	1.7548E-03	NA

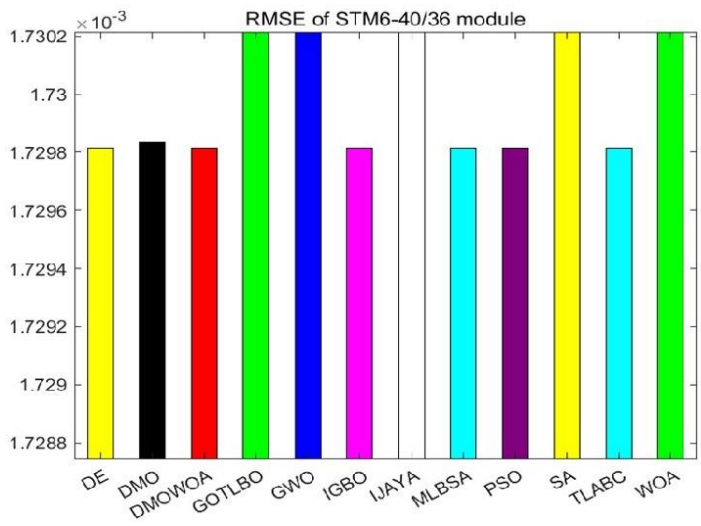

Figure 9. RMSE bar chart of STM6-40/36 module.

Table 9 summarizes the results of each algorithm for the STP6-120/36 module. Figure 10 presents the RMSE values of each algorithm for the STP6-120/36 module, indicating that DMOWOA, GOTLBO, MLBSA, TLABC, and IJAYA achieved the lowest RMSE values, followed by DMO, DE, PSO, and SA. GWO achieved the maximum RMSE.

Table 9. STP6-120/36 module parameters are extracted from each algorithm.

Method	I_{ph} (A)	I_{sd} (μA)	R_s (Ω)	R_{sh} (Ω)	a	RMSE	Runtime(s)
DMOWOA	7.4725388	2.3348795	0.1654074	799.416456	45.363577	**1.660060E-02**	**488.63**
DMO	7.4724523	2.3379871	0.1653883	805.843419	45.367562	1.660062E-02	502.95
WOA	7.4701126	2.5580463	0.1639131	1134.88340	45.639551	1.664355E-02	528.12
DE	7.4724591	2.3406457	0.1653676	806.593423	45.370987	1.660063E-02	529.53
SA	7.4713237	2.3449073	0.1653393	938.835347	45.501526	1.661138E-02	1002.39
PSO	7.4724061	1.7379582	0.1539021	811.83797	45.376454	1.660069E-02	518.40
GWO	7.4982327	7.5755745	0.1424305	934.576494	49.212400	1.925649E-02	566.35
IGBO [61]	7.472530	2.334995	0.165407	799.916580	45.363725	**1.660060E-02**	NA
GOTLBO [63]	7.472529	2.334887	0.004595	22.220503	1.260100	**1.660060E-02**	NA
MLBSA [27]	7.47253	2.3350	0.00459	22.21991	1.260103	**1.660060E-02**	NA
TLABC [27]	7.4725	2.3349	0.0046	22.2117	1.2601	**1.6601E-02**	NA
IJAYA [63]	7.47253	2.3350	0.00459	22.21809	1.260102	**1.660060E-02**	NA

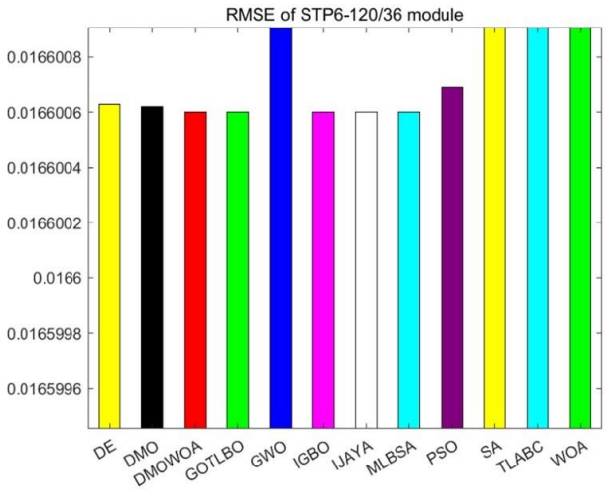

Figure 10. RMSE bar chart of STP6-120/36 module.

Table 10. Photowatt-PWP201 module: IAE of DMOWOA.

Item	Model data		Experiment current data		Experiment power data	
	V_M (V)	I_M (A)	I_E (A)	IAE_I (A)	P_E (W)	IAE_P (W)
1	0.1248	1.0315	1.029118847	0.00238115	0.12843403	0.00029717
2	1.8093	1.0300	1.027380741	0.00261926	1.85883997	0.00473903
3	3.3511	1.0260	1.025741449	0.00025855	3.43736217	0.00086643
4	4.7622	1.0220	1.024106793	0.00210679	4.87700137	0.01003297
5	6.0538	1.0180	1.022291430	0.00429143	6.18874786	0.02597946
6	7.2364	1.0155	1.019930298	0.00443030	7.38062361	0.03205941
7	8.3189	1.0140	1.016362718	0.00236272	8.45501981	0.01965521
8	9.3097	1.0100	1.010495764	0.00049576	9.40741241	0.00461541
9	10.2163	1.0035	1.000628591	0.00287141	10.22272187	0.02933518
10	11.0449	0.9880	0.984548016	0.00345198	10.87423438	0.03812682
11	11.8018	0.9630	0.959521338	0.00347866	11.32407893	0.04105447
12	12.4929	0.9255	0.922838511	0.00266149	11.52892923	0.03324972
13	13.1231	0.8725	0.872599390	0.00009939	11.45120905	0.00130430
14	13.6983	0.8075	0.807274025	0.00022597	11.05828178	0.00309547
15	14.2221	0.7265	0.728336268	0.00183627	10.35847124	0.02611559
16	14.6995	0.6345	0.637137811	0.00263781	9.36560725	0.03877450
17	15.1346	0.5345	0.536212884	0.00171288	8.11536751	0.02592381
18	15.5311	0.4275	0.429511145	0.00201115	6.67078054	0.03123529
19	15.8929	0.3185	0.318774291	0.00027429	5.06624793	0.00435928
20	16.2229	0.2085	0.207389294	0.00111071	3.36445578	0.01801887
21	16.5241	0.1010	0.096166930	0.00483307	1.58907197	0.07986213
22	16.7987	−0.0080	−0.008325661	0.00032566	−0.13986028	0.00547068
23	17.0499	−0.1110	−0.110936796	0.00006320	−1.89146128	0.00107762
24	17.2793	−0.2090	−0.209247621	0.00024762	−3.61565242	0.00427872
25	17.4885	−0.3030	−0.300863984	0.00213602	−5.26165978	0.03735572
SIAE				0.04892354		0.51688326

Table 11. STM6-40/36 module: IAE of DMOWOA.

Item	Model data		Experiment current data		Experiment power data	
	V_M (V)	I_M (A)	I_E (A)	IAE_I (A)	P_E (W)	IAE_P (W)
1	0.0000	1.6630	1.663458477	0.00045848	0.00000000	0.00000000
2	0.118	1.663	1.663252528	0.00025253	0.19626380	0.00002980
3	2.237	1.661	1.659551023	0.00144898	3.71241564	0.00324136
4	5.434	1.653	1.653914907	0.00091491	8.98737360	0.00497160
5	7.260	1.650	1.650566119	0.00056612	11.98311002	0.00411002
6	9.680	1.645	1.645430806	0.00043081	15.92777020	0.00417020
7	11.59	1.640	1.639233735	0.00076626	18.99871899	0.00888101
8	12.60	1.636	1.633712893	0.00228711	20.58478245	0.02881755
9	13.37	1.629	1.627286004	0.00171400	21.75681387	0.02291613
10	14.09	1.619	1.618313771	0.00068623	22.80204103	0.00966897
11	14.88	1.597	1.603090239	0.00609024	23.85398276	0.09062276
12	15.59	1.581	1.581588568	0.00058857	24.65696578	0.00917578
13	16.40	1.542	1.542330778	0.00033078	25.29422476	0.00542476
14	16.71	1.524	1.521192818	0.00280718	25.41913199	0.04690801
15	16.98	1.500	1.499194924	0.00080508	25.45632981	0.01367019
16	17.13	1.485	1.485275448	0.00027545	25.44276842	0.00471842
17	17.32	1.465	1.465654417	0.00065442	25.38513450	0.01133450
18	17.91	1.388	1.387589528	0.00041047	24.85172845	0.00735155
19	19.08	1.118	1.118391479	0.00039148	21.33890942	0.00746942
20	21.0200	0.0000	−0.000024852	0.00002485	−0.00052239	0.00052239
SIAE				0.02190395		0.28400442

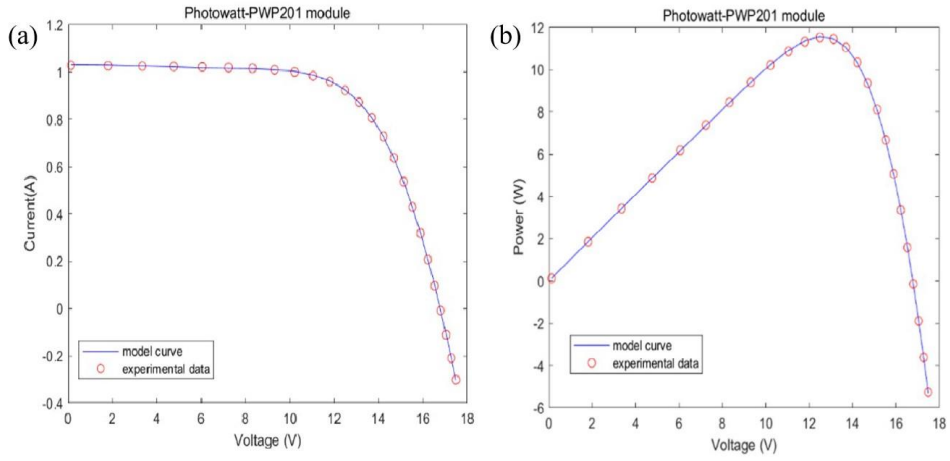

Figure 11. Comparison of experimental data and model data on Photowatt-PWP201 module: (a) I-V curve, (b) P-V curve.

The I-V and P-V curves of the Photowatt-PWP201 module are shown in Figure 11, and its IAE values are shown in Table 10. Table 10 reveals that the current-related IAE values remain below 4.83E-03, while power-related IAE values stay below 7.98E-02. Table 11 shows the IAE of the STM6-40/36

module calculated by DMOWOA, and Figure 12 shows the I-V and P-V curves. In Table 11, the current-related IAE values are all below 2.80E-03, and the power-related IAE values are all below 4.69E-02. Table 12 shows the IAE value of DMOWOA for the STP6-120/36 module, and Figure 13 shows the I-V and P-V curves of the STP6-120/36 module solved by DMOWOA. In Table 12, the current-related IAE values are all below 3.26E-02, and the power-related IAE values are all below 5.32E-01. The precision of the extracted parameters of DMOWOA be validated based on the data presented in both the table and figure.

Table 12. STP6-120/36 module: IAE of DMOWOA.

Item	Model data		Experiment current data		Experiment power data	
	V_M (V)	I_M (A)	I_E (A)	IAE_I (A)	P_E (W)	IAE_P (W)
1	19.2100	0.0000	0.002281450	0.00228145	0.04382665	0.04382665
2	17.65	3.83	3.833350655	0.00335065	67.65863906	0.05913906
3	17.41	4.29	4.267341161	0.02265884	74.29440961	0.39449039
4	17.25	4.56	4.541152144	0.01884786	78.33487448	0.32512552
5	17.10	4.79	4.784403781	0.00559622	81.81330466	0.09569534
6	16.90	5.07	5.085581533	0.01558153	85.94632791	0.26332791
7	16.76	5.27	5.274825808	0.00482581	88.40608054	0.08088054
8	16.34	5.75	5.782600330	0.03260033	94.48768939	0.53268939
9	16.08	6.00	6.044320443	0.04432044	97.19267272	0.71267272
10	15.71	6.36	6.347122775	0.01287723	99.71329880	0.20230120
11	15.39	6.58	6.566551247	0.01344875	101.05922369	0.20697631
12	14.93	6.83	6.813611664	0.01638834	101.72722214	0.24467786
13	14.58	6.97	6.957709845	0.01229015	101.44340954	0.17919046
14	14.17	7.10	7.087575446	0.01242455	100.43094407	0.17605593
15	13.59	7.23	7.217384025	0.01261598	98.08424890	0.17145110
16	13.16	7.29	7.283998507	0.00600149	95.85742035	0.07897965
17	12.74	7.34	7.331344298	0.00865570	93.40132636	0.11027364
18	12.36	7.37	7.363181985	0.00681802	91.00892933	0.08427067
19	11.81	7.38	7.395998685	0.01599869	87.34674447	0.18894447
20	11.17	7.41	7.420314779	0.01031478	82.88491608	0.11521608
21	10.32	7.44	7.439089236	0.00091076	76.77140092	0.00939908
22	9.740	7.42	7.446761859	0.02676186	72.53146051	0.26066051
23	9.060	7.45	7.452540600	0.00254060	67.52001784	0.02301784
24	0.0000	7.4800	7.470986525	0.00901348	0.00000000	0.00000000
SIAE				0.31712351		4.55926232

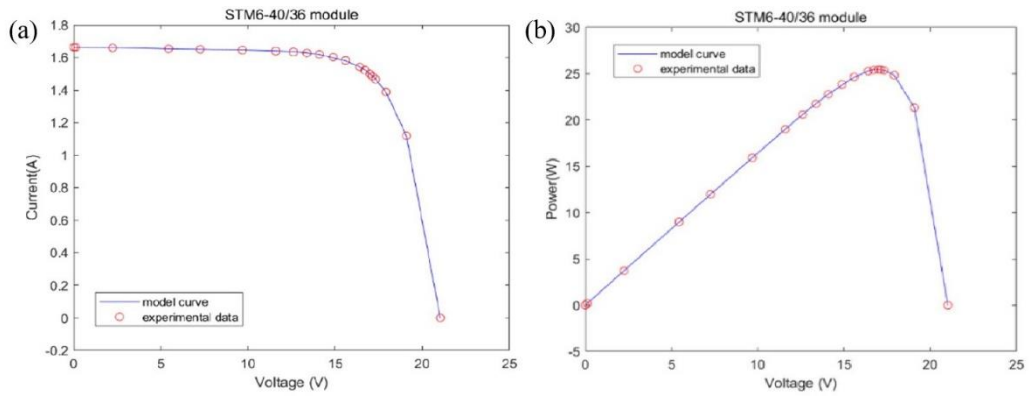

Figure 12. Comparison of experimental data and model data on STM6-40/36 module: (a) I-V curve, (b) P-V curve.

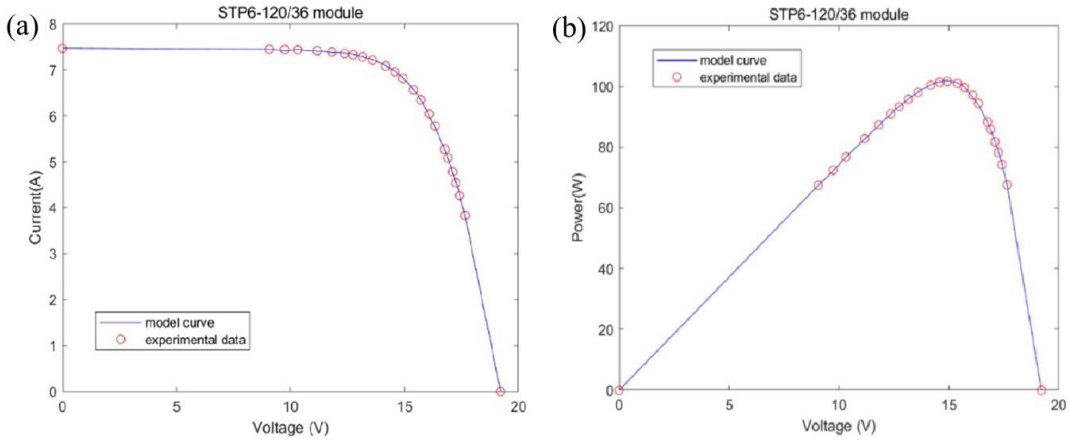

Figure 13. Comparison of experimental data and model data on STP6-120/36 module: (a) I-V curve, (b) P-V curve.

5.4. Statistical results and convergence curves

In this section, the experimental results and convergence curves of different algorithms for solving the parameters of the photovoltaic model are presented and analyzed. Table 13 shows the minimum, maximum, average, and standard deviation of RMSE for PV models solved by different algorithms. All of the algorithms were run independently 30 times. In Table 13, Min represents the lowest RMSE value, Max represents the highest RMSE value, Mean represents the average RMSE value, and SD represents the algorithm's stability. The lowest RMSE values for each module are in bold. Due to the lack of specific experimental data in the literature, comparisons are limited to four basic statistical indicators, consistent with the methods of comparison in the literature. The statistical analysis of the proposed methodology is limited.

For the single diode model, according to Table 13, DMOWOA achieves the lowest RMSE value, while DMO excels across minimum, maximum, and average RMSE. Furthermore, MLBSA exhibits the lowest standard deviation, indicating consistent performance.

Table 13. Statistical results of different algorithms for solving photovoltaic models.

PV model	Method	RMSE			
		Min	Max	Mean	SD
SDM	DMOWOA	**9.860219E-04**	9.964806E-04	9.870776E-04	3.188117E-06
	DMO	**9.860219E-04**	**9.860226E-04**	**9.860221E-04**	1.807731E-10
	WOA	1.107616E-03	4.578496E-02	7.102568E-03	1.236875E-02
	DE	**9.860219E-04**	1.438509E-03	1.001135E-03	8.260681E-05
	SA	1.049349E-03	2.246603E-03	1.881534E-03	3.583774E-04
	PSO	9.860259E-04	9.861631E-04	9.860669E-04	3.742250E-08
	GWO	1.005399E-03	3.815095E-02	6.366746E-03	1.267456E-02
	IGBO [61]	**9.860219E-04**	9.864489E-04	9.860444E-04	8.838088E-08
	GOTLBO [34]	9.87442E-04	1.98244E-03	1.33488E-03	2.99407E-04
	MLBSA [37]	**9.8602E-04**	**9.8602E-04**	**9.8602E-04**	**9.1461E-12**
	TLABC [32]	**9.86022E-04**	1.03970E-03	9.98523E-04	1.86022E-05
	IJAYA [35]	9.8603E-04	1.0622E-03	9.9204E-04	1.4033E-05
DDM	DMOWOA	**9.824894E-04**	1.409552E-03	9.990270E-04	7.755141E-05
	DMO	9.857786E-04	9.881073E-04	**9.863471E-04**	**5.804664E-07**
	WOA	1.114960E-03	4.118252E-02	8.491764E-03	1.326261E-02
	DE	9.860225E-04	1.106283E-03	1.011058E-03	2.937064E-05
	SA	9.880796E-04	2.206404E-03	1.335049E-03	2.916275E-04
	PSO	9.835519E-04	9.892810E-04	9.860059E-04	1.062786E-06
	GWO	1.010862E-03	3.808132E-02	2.65525E-03	6.70687E-03
	IGBO [61]	9.826373E-04	1.370334E-03	1.026447E-03	1.131003E-03
	GOTLBO [34]	9.83177E-04	1.78774E-03	1.24360E-03	2.09115E-04
	MLBSA [37]	**9.8249E-04**	**9.8798E-04**	9.8518E-04	1.3482E-06
	TLABC [32]	9.84145E-04	1.50482E-03	1.05553E-03	1.55034E-04
	IJAYA [35]	9.8293E-04	1.0622E-03	9.9204E-04	1.4033E-05
Photowatt-PWP201	DMOWOA	**2.425075E-03**	2.608133E-03	2.528525E-03	9.102414E-05
	DMO	2.425081E-03	**2.425201E-03**	**2.425115E-03**	**2.670061E-08**
	WOA	2.604337E-03	2.742507E-01	5.317646E-02	1.020819E-01
	DE	**2.425075E-03**	2.425715E-03	2.425124E-03	1.212543E-07
	SA	2.453717E-03	4.271164E-03	2.647786E-03	3.345887E-04
	PSO	2.425089E-03	2.478674E-03	2.428055E-03	9.703640E-06
	GWO	2.460404E-03	2.888445E-03	2.647212E-03	1.062403E-04
	IGBO [61]	**2.425075E-03**	2.430055E-03	2.425573E-03	1.574886E-06
	GOTLBO [63]	2.427130E-03	2.574944E-03	2.469844E-03	3.1248E-05
	MLBSA [37]	**2.425075E-03**	2.425312E-03	2.425084E-03	4.336794E-08
	TLABC [63]	**2.42507E-03**	2.44584E-03	2.42647E-03	3.99568E-06
	IJAYA [35]	**2.4251E-03**	2.4393E-03	2.4289E-03	3.7755E-06
STM6-40/36	DMOWOA	**1.729814E-03**	3.585698E-02	3.419714E-03	6.185169E-03
	DMO	1.729834E-03	1.729963E-03	**1.729883E-03**	3.131366E-08
	WOA	1.884297E-03	7.355741E-03	3.726836E-03	1.181472E-03
	DE	1.729815E-03	1.733418E-03	1.730283E-03	6.743370E-07

Continued on next page

PV model	Method	RMSE			
		Min	Max	Mean	SD
STM6-40/36	SA	2.572751E-03	3.197710E-03	3.025829E-03	1.597912E-04
	PSO	**1.729814E-03**	1.734963E-03	1.730976E-03	1.294072E-06
	GWO	2.494334E-03	3.376361E-03	3.291131E-03	1.616028E-04
	IGBO [61]	**1.729814E-03**	**1.729840E-03**	1.729816E-03	**8.152893E-09**
	GOTLBO [63]	2.0281E-03	3.3307E-03	2.5944E-03	3.696259E-04
	MLBSA [27]	**1.7298E-03**	2.7932E-03	1.7788E-03	1.968672E-04
	TLABC [27]	**1.7298E-03**	6.5053E-03	2.1827E-03	9.22E-04
	IJAYA [63]	**1.7298E-03**	3.3248E-02	2.7814E-03	5.754224E-03
STP6-120/36	DMOWOA	**1.660060E-02**	2.846505E-02	1.784015E-02	3.673024E-03
	DMO	1.660062E-02	**1.660071E-02**	**1.660066E-02**	**2.601586E-08**
	WOA	1.664356E-02	3.558664E-02	2.582329E-02	5.148497E-03
	DE	1.660063E-02	1.664268E-02	1.664078E-02	7.583427E-06
	SA	1.661138E-02	2.593994E-02	2.380168E-02	1.903130E-03
	PSO	1.660069E-02	1.664214E-02	1.662816E-02	1.878813E-05
	GWO	1.925649E-02	1.413122E-02	7.216812E-02	2.532743E-01
	IGBO [61]	**1.660060E-02**	1.664210E-02	1.661328E-02	1.980840E-05
	GOTLBO [63]	1.7987E-02	3.6968E-02	2.5473E-02	5.612662E-03
	MLBSA [27]	**1.6601E-02**	1.8269E-02	1.6731E-02	3.01E-04
	TLABC [27]	**1.6601E-02**	2.1497E-02	1.6963E-02	9.47E-04
	IJAYA [63]	**1.66006E-02**	1.7155E + 00	1.3486E-01	4.298527E-01

In the double diode model analysis, Table 13 reveals that DMOWOA and MLBSA share the lowest minimum RMSE. Notably, DMO achieves the lowest mean and standard deviation, demonstrating overall stability and accuracy. Finally, MLBSA has the lowest maximum RMSE, suggesting its potential for robust performance across diverse scenarios.

For the Photowatt-PWP201 module, according to Table 13, DMOWOA achieves the lowest minimum RMSE. Interestingly, DMO dominates in all three categories, boasting the lowest maximum mean square error, root mean square error, and standard deviation.

Table 13 shows that DMOWOA obtains the lowest value in the ‘Min’ category for both the STM6-40/36 and STP6-120/36 modules. For the STM6-40/36 module, IGBO also achieves the lowest values in the ‘Max’ and ‘SD’ categories, while DMO achieves the lowest value in the ‘Mean’ category. For the STP6-120/36 module, DMOWOA performs well in all categories, demonstrating its strong competitiveness. DMO achieves the lowest values in the ‘Max’, ‘Mean’, and ‘SD’ categories for this module.

A visual inspection of Figure 14 suggests that DMOWOA achieves the fastest convergence speed. DMOWOA’s performance is particularly noteworthy for the DDM and STM6-40/36 modules, where it converges to the optimal solution in the fewest iterations. Based on the results, DMOWOA is a promising candidate for the robust, efficient, and accurate extraction of photovoltaic model parameters.

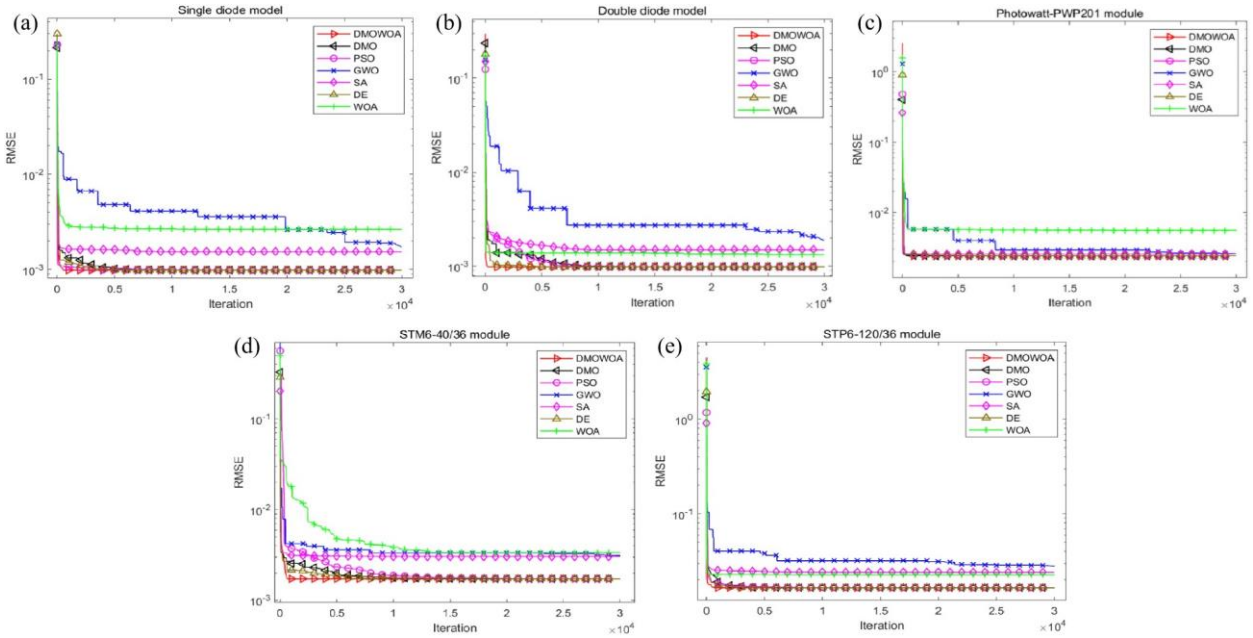

Figure 14. Convergence curves: (a) single diode model, (b) double diode model, (c) Photowatt-PWP201 module, (d) STM6-40/36 module, (e) STP6-120/36 module.

5.5. Comparison with literature

This section compares the experimental results of DMOWOA for various PV models with those reported in the literature. Table 3 compares the performance of DMOWOA, IGBO [61], GOTLBO [34], MLBSA [37], TLABC [35], and IJAYA [35] in solving the SDM. DMOWOA achieves the lowest RMSE value among all algorithms in Table 3. In Table 5, DMOWOA and MLBSA achieve the lowest RMSE values, followed by IGBO [61], IJAYA [35], GOTLBO [34], and TLABC [35].

The analysis findings for various photovoltaic models are proposed as follows. For the Photowatt-PWP201 module, in Table 7, DMOWOA and IGBO [61], GOTLBO [63], MLBSA [37], TLABC [63] all got the minimum RMSE, and the worst was IJAYA. In Table 8, the results of extracting parameters of the STM6-40/36 module are shown. DMOWOA and IGBO [61], MLBSA [27], TLABC [27], IJAYA [63] all obtained the minimum RMSE, and GOTLBO [63] got the maximum. For the STP6-120/36 module, in Table 9, DMOWOA and IGBO [61], MLBSA [27], TLABC [27], IJAYA [63] all obtained the minimum RMSE, and GOTLBO [63] obtained the maximum RMSE.

Overall, DMOWOA achieved the lowest RMSE value in all models. This is consistent with the results of previous studies and even outperforms other methods in some models. Therefore, DMOWOA is a promising candidate for efficient, accurate, and alternative PV model parameter extraction.

6. Conclusions and future work

The accurate extraction of photovoltaic parameters plays a key role in the design and efficient operation of photovoltaic systems. In this study, combining the DMO and the WOA, an adaptive dwarf mongoose optimization algorithm of the hybrid whale algorithm is proposed. In this method, the integration of the search phase of dwarf mongoose and the bubble net attack mode of the whale

optimization algorithm was employed to enhance its capability to escape local optima. Reconcile exploration and exploitation by incorporating inertia weights. The proposed algorithm is employed to solve various photovoltaic models to validate its performance. The experimental results are compared with other established algorithms. The test data demonstrates that DMOWOA can quickly and accurately obtain results and has strong competitiveness in accuracy and reliability. The proposed DMOWOA can serve as an efficient alternative approach for addressing the parameter estimation of photovoltaic models. However, the proposed DMOWOA cannot solve multi-objective optimization problems. In future work, the proposed algorithm can be enhanced by incorporating other methodologies, thereby addressing various optimization problems within the energy domain.

Use of AI tools declaration

The authors declare they have not used Artificial Intelligence (AI) tools in the creation of this article.

Acknowledgments

This work was supported by the National Natural Science Foundation of China (U21A20464), the Innovation Project of Guangxi Graduate Education (YCSW2023259).

Conflict of interest

The authors declare no conflict of interest.

Author contributions

Shijian Chen carried out the DMOWOA algorithm studies, participated in the drafted the manuscript. Yongquan Zhou carried out the review & editing; Qifang Luo carried out the DMOWOA test. All authors read and approved the final manuscript.

References

1. Shindell D, Smith CJ (2019) Climate and air-quality benefits of a realistic phase-out of fossil fuels. *Nature* 573: 408–411. https://doi.org/10.1038/s41586-019-1554-z
2. Hu G, Wang J, Su Z, et al. (2019) Performance evaluation of twin piezoelectric wind energy harvesters under mutual interference. *Appl Phys Lett* 115: 073901. https://doi.org/10.1063/1.5109457
3. Cabrera P, Carta JA, Lund H, et al. (2021) Large-scale optimal integration of wind and solar photovoltaic power in water-energy systems on islands. *Energy Convers Manage* 235: 113982. https://doi.org/10.1016/j.enconman.2021.113982
4. Askarzadeh A, Rezazadeh A (2013) Artificial bee swarm optimization algorithm for parameters identification of solar cell models. *Appl Energy* 102: 943–949. https://doi.org/10.1016/j.apenergy.2012.09.052

5. Jordehi AR (2018) Enhanced leader particle swarm optimisation (ELPSO): An efficient algorithm for parameter estimation of photovoltaic (PV) cells and modules. *Sol Energy* 159: 78–87. https://doi.org/10.1016/j.solener.2017.10.063
6. Alam DF, Yousri DA, Eteiba MB (2015) Flower pollination algorithm based solar PV parameter estimation. *Energy Convers Manage* 101: 410–422. https://doi.org/10.1016/j.enconman.2015.05.074
7. Humada AM, Hojabri M, Mekhilef S, et al (2016) Solar cell parameters extraction based on single and double-diode models: A review. *Renewable Sustainable Energy Rev* 56: 494–509. https://doi.org/10.1016/j.rser.2015.11.051
8. Chin VJ, Salam Z, Ishaque K (2015) Cell modelling and model parameters estimation techniques for photovoltaic simulator application: A review. *Appl Energy* 154: 500–519. https://doi.org/10.1016/j.apenergy.2015.05.035
9. Li S, Gong W, Gu Q (2021) A comprehensive survey on meta-heuristic algorithms for parameter extraction of photovoltaic models. *Renewable Sustainable Energy Rev* 141: 110828. https://doi.org/10.1016/j.rser.2021.110828
10. Chan DSH, Phang JCH (1987) Analytical methods for the extraction of solar-cell single-and double-diode model parameters from IV characteristics. *IEEE Trans Electron Devices* 34: 286–293. https://doi.org/10.1109/T-ED.1987.22920
11. Adeel M, Hassan AK, Sher HA, et al. (2021) A grade point average assessment of analytical and numerical methods for parameter extraction of a practical PV device. *Renewable Sustainable Energy Rev* 142: 110826. https://doi.org/10.1016/j.rser.2021.110826
12. Easwarakhanthan T, Bottin J, Bouhouch I, et al. (1986) Nonlinear minimization algorithm for determining the solar cell parameters with microcomputers. *Int J Sol Energy* 4: 1–12. https://doi.org/10.1080/01425918608909835
13. Nassar-Eddine I, Obbadi A, Errami Y, et al. (2016) Parameter estimation of photovoltaic modules using iterative method and the Lambert W function: A comparative study. *Energy Convers Manage* 119: 37–48. https://doi.org/10.1016/j.enconman.2016.04.030
14. Et-Torabi K, Nassar-Eddine I, Obbadi A, et al. (2017) Parameters estimation of the single and double diode photovoltaic models using a Gauss-Seidel algorithm and analytical method: A comparative study. *Energy Convers Manage* 148: 1041–1054. https://doi.org/10.1016/j.enconman.2017.06.064
15. Chan DSH, Phillips JR, Phang JCH (1986) A comparative study of extraction methods for solar cell model parameters. *Solid-State Electron* 29: 329–337. https://doi.org/10.1016/0038-1101(86)90212-1
16. Gao S, Yu Y, Wang Y, et al. (2019) Chaotic local search-based differential evolution algorithms for optimization. *IEEE Trans Syst Man Cybern: Syst* 51: 3954–3967. https://doi.org/10.1109/TSMC.2019.2956121
17. Hansen N, Müller SD, Koumoutsakos P (2003) Reducing the time complexity of the derandomized evolution strategy with covariance matrix adaptation (CMA-ES). *J Evol Comput* 11: 1–18. https://doi.org/10.1162/106365603321828970
18. Guzman R, Oliveira R, Ramos F (2020) Heteroscedastic bayesian optimisation for stochastic model predictive control. *IEEE Rob Autom Lett* 6: 56–63. https://doi.org/10.1109/LRA.2020.3028830

19. Zagrouba M, Sellami A, Bouaïcha M, et al. (2010) Identification of PV solar cells and modules parameters using the genetic algorithms: Application to maximum power extraction. *Sol Energy* 84: 860–866. https://doi.org/10.1016/j.solener.2010.02.012
20. Hu Z, Gong W, Li S (2021) Reinforcement learning-based differential evolution for parameters extraction of photovoltaic models. *Energy Rep* 7: 916–928. https://doi.org/10.1016/j.egyr.2021.01.096
21. Ye M, Wang X, Xu Y (2009) Parameter extraction of solar cells using particle swarm optimization. *J Appl Phys* 105: 094502. https://doi.org/10.1063/1.3122082
22. El-Naggar KM, AlRashidi MR, AlHajri MF, et al. (2012) Simulated annealing algorithm for photovoltaic parameters identification. *Sol Energy* 86: 266–274. https://doi.org/10.1016/j.solener.2011.09.032
23. Allam D, Yousri DA, Eteiba MB (2016) Parameters extraction of the three diode model for the multi-crystalline solar cell/module using Moth-Flame Optimization Algorithm. *Energy Convers Manage* 123: 535–548. https://doi.org/10.1016/j.enconman.2016.06.052
24. Oliva D, Cuevas E, Pajares G (2014) Parameter identification of solar cells using artificial bee colony optimization. *Energy* 72: 93–102. https://doi.org/10.1016/j.energy.2014.05.011
25. Yu K, Chen X, Wang X, et al. (2017) Parameters identification of photovoltaic models using self-adaptive teaching-learning-based optimization. *Energy Convers Manage* 145: 233–246. https://doi.org/10.1016/j.enconman.2017.04.054
26. Zhang Y, Ma M, Jin Z (2020) Comprehensive learning Jaya algorithm for parameter extraction of photovoltaic models. *Energy* 211: 118644. https://doi.org/10.1016/j.energy.2020.118644
27. Li S, Gu Q, Gong W, et al. (2020) An enhanced adaptive differential evolution algorithm for parameter extraction of photovoltaic models. *Energy Convers Manage* 205: 112443. https://doi.org/10.1016/j.enconman.2019.112443
28. Merchaoui M, Sakly A, Mimouni MF (2018) Particle swarm optimisation with adaptive mutation strategy for photovoltaic solar cell/module parameter extraction. *Energy Convers Manage* 175: 151–163. https://doi.org/10.1016/j.enconman.2018.08.081
29. Ishaque K, Salam Z (2011) An improved modeling method to determine the model parameters of photovoltaic (PV) modules using differential evolution (DE). *Sol Energy* 85: 2349–2359. https://doi.org/10.1016/j.solener.2011.06.025
30. Xiong G, Zhang J, Yuan X, et al. (2018) Parameter extraction of solar photovoltaic models by means of a hybrid differential evolution with whale optimization algorithm. *Sol Energy* 176: 742–761. https://doi.org/10.1016/j.solener.2018.10.050
31. Jiang LL, Maskell DL, Patra JC (2013) Parameter estimation of solar cells and modules using an improved adaptive differential evolution algorithm. *Appl Energy* 112: 185–193. https://doi.org/10.1016/j.apenergy.2013.06.004
32. Chen X, Xu B, Mei C, et al. (2018) Teaching-learning-based artificial bee colony for solar photovoltaic parameter estimation. *Appl Energy* 212: 1578–1588. https://doi.org/10.1016/j.apenergy.2017.12.115
33. Niu Q, Zhang H, Li K (2014) An improved TLBO with elite strategy for parameters identification of PEM fuel cell and solar cell models. *Int J Hydrogen Energy* 39: 3837–3854. https://doi.org/10.1016/j.ijhydene.2013.12.110

34. Chen X, Yu K, Du W, et al. (2016) Parameters identification of solar cell models using generalized oppositional teaching learning based optimization. *Energy* 99: 170–180. https://doi.org/10.1016/j.energy.2016.01.052
35. Yu K, Liang JJ, Qu BY, et al. (2017) Parameters identification of photovoltaic models using an improved JAYA optimization algorithm. *Energy Convers Manage* 150: 742–753. https://doi.org/10.1016/j.enconman.2017.08.063
36. Yu K, Qu B, Yue C, et al. (2019) A performance-guided JAYA algorithm for parameters identification of photovoltaic cell and module. *Appl Energy* 237: 241–257. https://doi.org/10.1016/j.apenergy.2019.01.008
37. Yu K, Liang JJ, Qu BY, et al. (2018) Multiple learning backtracking search algorithm for estimating parameters of photovoltaic models. *Appl Energy* 226: 408–422. https://doi.org/10.1016/j.apenergy.2018.06.010
38. Abdel-Basset M, El-Shahat D, Sallam KM, et al. (2022) Parameter extraction of photovoltaic models using a memory-based improved gorilla troops optimizer. *Energy Convers Manage* 252: 115134. https://doi.org/10.1016/j.enconman.2021.115134
39. Xiong G, Zhang J, Shi D, et al. (2018) Parameter extraction of solar photovoltaic models using an improved whale optimization algorithm. *Energy Convers Manage* 174: 388–405. https://doi.org/10.1016/j.enconman.2018.08.053
40. Oliva D, Abd El Aziz M, Hassanien AE (2017) Parameter estimation of photovoltaic cells using an improved chaotic whale optimization algorithm. *Appl Energy* 200: 141–154. https://doi.org/10.1016/j.apenergy.2017.05.029
41. Pan JS, Tian AQ, Snášel V, et al. (2022) Maximum power point tracking and parameter estimation for multiple-photovoltaic arrays based on enhanced pigeon-inspired optimization with Taguchi method. *Energy* 251: 123863. https://doi.org/10.1016/j.energy.2022.123863
42. Wang X, Chu SC, Snášel V, et al. (2021) A two-phase quasi-affine transformation evolution with feedback for parameter identification of photovoltaic models. *Appl Soft Comput* 113: 107978. https://doi.org/10.1016/j.asoc.2021.107978
43. Yu Y, Gao S, Zhou MC, et al. (2022) Scale-free network-based differential evolution to solve function optimization and parameter estimation of photovoltaic models. *Swarm Evol Comput* 74: 101142. https://doi.org/10.1016/j.swevo.2022.101142
44. Yu Y, Wang K, Zhang T, et al. (2022) A population diversity-controlled differential evolution for parameter estimation of solar photovoltaic models. *Sustainable Energy Technol Assess* 51: 101938. https://doi.org/10.1016/j.seta.2021.101938
45. Gao S, Wang K, Tao S, et al. (2021) A state-of-the-art differential evolution algorithm for parameter estimation of solar photovoltaic models. *Energy Convers Manage* 230: 113784. https://doi.org/10.1016/j.enconman.2020.113784
46. Das S, Suganthan PN (2010) Differential evolution: A survey of the state-of-the-art. *IEEE Trans Evol Comput* 15: 4–31. https://doi.org/10.1109/TEVC.2010.2059031
47. Agushaka JO, Ezugwu AE, Abualigah L (2022) Dwarf mongoose optimization algorithm. *Comput Methods Appl Mech Eng* 391: 114570. https://doi.org/10.1016/j.cma.2022.114570
48. Mirjalili S, Lewis A (2016) The whale optimization algorithm. *Adv Eng Software* 95: 51–67. https://doi.org/10.1016/j.advengsoft.2016.01.008

49. AlRashidi MR, AlHajri MF, El-Naggar KM, et al. (2011) A new estimation approach for determining the I-V characteristics of solar cells. *Sol Energy* 85: 1543–1550. https://doi.org/10.1016/j.solener.2011.04.013
50. Marti A, Balenzategui JL, Reyna RF (1997) Photon recycling and Shockley's diode equation. *J Appl Phys* 82: 4067. https://doi.org/10.1063/1.365717
51. Premkumar M, Jangir P, Sowmya R, et al. (2021) Enhanced chaotic JAYA algorithm for parameter estimation of photovoltaic cell/modules. *ISA Trans* 116: 139–166. https://doi.org/10.1016/j.isatra.2021.01.045
52. Ram JP, Babu TS, Dragicevic T, et al. (2017) A new hybrid bee pollinator flower pollination algorithm for solar PV parameter estimation. *Energy Convers Manage* 135: 463–476. https://doi.org/10.1016/j.enconman.2016.12.082
53. Abdel-Basset M, Mohamed R, Chakrabortty RK, et al. (2021) An efficient teaching-learning-based optimization algorithm for parameters identification of photovoltaic models: Analysis and validations. *Energy Convers Manage* 227: 113614. https://doi.org/10.1016/j.enconman.2020.113614
54. Nickabadi A, Ebadzadeh MM, Safabakhsh R (2011) A novel particle swarm optimization algorithm with adaptive inertia weight. *Appl Soft Comput* 11: 3658–3670. https://doi.org/10.1016/j.asoc.2011.01.037
55. Feng Y, Teng GF, Wang AX, et al. (2007) Chaotic inertia weight in particle swarm optimization. *Second International Conference on Innovative Computing, Informatio and Control*, Kumamoto, Japan, 475. https://doi.org/10.1109/ICICIC.2007.209
56. Feng Y, Yao YM, Wang AX (2007) Comparing with chaotic inertia weights in particle swarm optimization. *2007 International Conference on Machine Learning and Cybernetics*, Hong Kong, China. https://doi.org/10.1109/ICMLC.2007.4370164
57. Cai Z, Yang X, Zhou MC, et al. (2023) Toward explicit control between exploration and exploitation in evolutionary algorithms: A case study of differential evolution. *Inf Sci* 649: 119656. https://doi.org/10.1016/j.ins.2023.119656
58. Tong NT, Pora W (2016) A parameter extraction technique exploiting intrinsic properties of solar cells. *Appl Energy* 176: 104–115. https://doi.org/10.1016/j.apenergy.2016.05.064
59. Storn R, Price K (1997) Differential evolution—A simple and efficient heuristic for global optimization over continuous spaces. *J Global Optim* 11: 341–359. https://doi.org/10.1023/A:1008202821328
60. Kennedy J, Eberhart R (1995) Particle swarm optimization. Proceedings of ICNN'95—International Conference on Neural Networks, IEEE. http://dx.doi.org/10.1109/icnn.1995.488968
61. Jiang Y, Luo Q, Zhou Y (2022) Improved gradient-based optimizer for parameters extraction of photovoltaic models. *J IET Renewable Power Generation* 16: 1602–1622. https://doi.org/10.1049/rpg2.12465
62. Li S, Gong W, Yan X, et al. (2019) Parameter extraction of photovoltaic models using an improved teaching-learning-based optimization. *Energy Convers Manage* 186: 293–305. https://doi.org/10.1016/j.enconman.2019.02.048
63. Liang J, Ge S, Qu B, et al. (2020) Classified perturbation mutation based particle swarm optimization algorithm for parameters extraction of photovoltaic models. *Energy Convers Manage* 203: 112138. https://doi.org/10.1016/j.enconman.2019.112138

64. Mirjalili S, Mirjalili SM, Lewis A (2014) Grey wolf optimizer. *Adv Eng Software* 69: 46–61. https://doi.org/10.1016/j.advengsoft.2013.12.007

AIMS Press